INVESTIGATION OF NOVEL DEVICES USED FOR PULSED LASER SYSTEM

TANG CHUN YIN

M.Phil

The Hong Kong Polytechnic University

2017

The Hong Kong Polytechnic University

Department of Applied Physics

INVESTIGATION OF NOVEL DEVICES USED FOR PULSED LASER SYSTEM

Tang Chun Yin

A thesis submitted in partial fulfillment of the requirements for the degree of Master of Philosophy

May 2016

CERTIFICATE OF ORIGINALITY

I hereby declare that this thesis is my own work and that, to the best of my knowledge and belief, it reproduces no material previously published or written, nor material that has been accepted for the award of any other degree or diploma, except where due acknowledgment has been made in the text.

_____

Tang Chun Yin

Abstract

With my main MPhil research focus being on the development of novel materials and devices that can potentially be integrated into the laser photonic system, I have started my research work on developing electrically tunable liquid lensed fiber that can be potentially used within the microfluidic biomedical sensors, or as optical switcher inserted within the laser cavity to serve as active laser Q-switcher. The novel functional microfluidic device investigated is a liquid lensed optical fiber with controllable focusing power. By filling water into a hollow Teflon-AF optical fiber and applying electrical field on the fiber tip, we can vary the shape and radius of curvature of the liquid lens on the fiber tip. By controlling the electric field across it, the shape, radius of curvature and focusing power of the formed liquid lens on the fiber tip can be varied. The experiment has successfully demonstrated a variation of focal length from 0.628mm to 0.111mm responding to the change of applied voltage from 0V to 3 kV (L = 2mm) for the Teflon AF fiber. Furthermore, by applying voltage higher than 2.6kV, parabolic shape of the liquid lens has been created, which can be a simple and practical method to produce micron sized parabolic lensed fiber compared to traditional mechanical polishing technique.

Passive mode-locked laser is typically achieved by the Semiconductor Saturable

absorber Mirror, SESAM, which is produced by expensive and complicated metal organic chemical vapor deposition method. Therefore, I have investigated the fabrication technology of saturable absorber for mode locking laser application during my MPhil study. Carbon based single wall carbon nanotube (SWCNT), saturable absorber, a promising material with the capability of producing stable passive mode-locking in the high power laser cavity over a wide operational wavelength range. This study has successfully demonstrated the high-power mode locking laser system operating at 1 micron by using SWCNT-based absorbers fabricated by dip coating method. The proposed materials and fabrication method is practical, simple and cost effective for fabricating SWCNT saturable absorber. Different from traditional spray or spin-coating deposition method, relatively uniform and large surface area SWCNT thin film (greater than $1cm^2$) is successfully coated on quartz plate to form a transmission type saturable absorber. By adjusting the dip coating parameters involving the concentration of the dip coating suspension, withdrawn speed and environment conditions (Temperature or relatively humidity), the initial transmission ratio of the fabricated absorber sample can be changed by 12%. The demonstrated high power Nd:YVO_4 mode-locked laser operating at 1064nm have maximum output power up to 2.7W, with the 167 MHz repetition

rate and 3.1 ps pulse duration, respectively. The calculated output pulse energy and peak power are 16.1 nJ and 5.2 kW, respectively.

List of publications

Publications overview: 9 journals papers published, 6 conference presentation.

1. **C. Y. Tang,** Y. Chai, H. Long, L. Tao, L. H. Zeng, Y. H. Tsang, L. Zhang, and X. Lin, "High-power passively mode-locked Nd:YVO_4 laser using SWCNT saturable absorber fabricated by dip coating method," Opt. Exp. 23(4), 4880-4886(2015).
2. **C. Y. Tang**, X. Zhang, Y. Chai, L. Hui, L. Tao, and Y. H. Tsang," Controllable parabolic lensed liquid-core optical fiber by using electrostatic force," Opt. Exp. 22(17), 20948-20953(2014).
3. H. Long, L. Tao, **C. Y. Tang**, B. Zhou, Y. D. Zhao, L. H. Zeng, S. F. Yu , S. P. Lau, Y. Chai, and Y. H. Tsang, " Tuning nonlinear optical absorption properties of WS_2 nanosheets, " Nanoscale, 7, 17771-17777, (2015).
4. H. Long, L. Tao, **C. Y. Tang**, H.-Y. Tam, Q. Wen and Y. H. Tsang, "Effect of laser illumination on the morphology and optical property of few-layer MoS_2 nanosheet in NMP and PMMA", Journal of materials chemistry C(4), 678-683,(2016).
5. L. Zeng, L. Tao, **C. Y. Tang**, B. Zhou, H. Long, C. Yang, S. P. Lau, Y. H.

Tsang, “High-responsivity UV-Vis Photodetector Based on Transferable WS_2 Film Deposited by Magnetron Sputtering”, Sci Rep. (6) 20343, (2016).

6. L. Tao, B. Zhou, W. Jin, Y. Chai, **C. Y. Tang**, and Y. H. Tsang, "Improved multiphoton ultraviolet up conversion photoluminescence in ultra small core-shell nanocrystals," Optics Letters, 39(21), 6265-6268 (2014).
7. L. Zeng, C. Xie, L. Tao, H. Long, **C. Y. Tang**, Y. H. Tsang, and J. Jie, "Bilayer graphene-based surface passivation enhanced nano structured self-powered near-infrared photodetector," Optics Express, 2(4), .4839-4846 (2015).
8. C. H. Mak, C. Liao, Y. Fu, M. Zhang, **C. Y. Tang**, Y. H. Tsang, H. L. W. Chan and F. Yan, "Highly-sensitive epinephrine sensors based on organic electrochemical transistors" Journal of materials chemistry C, **3**, 6532-6538(2015).
9. H. Fang, Z. Lin, X. Wang, **C. Y. Tang**, Y. Chen, F. Zhang, Y. Chai, Q Li, Q. F. Yan, H.L.W. Chan, and J.-Y. Dai," Infrared light-gated MoS_2 field effect transistor" Opt. Exp. (23)25, 31908-31914(2015).

Conferences:

1. **C. Y. Tang**, L.-H. Zeng, H. Long, L.-L. Tao , C.-C. Huang, D. W. Hewak, Y. H. Tsang, "Study of TMDs nanosheets based saturable absorber used for Q-switching and mode lock laser system ",The EMN Bangkok Meeting 2015, November 2015 (**Invited talk**)

2. G. Bai, **C.-Y. Tang**, K. L. Jim, X. Zhang, and Y. H. Tsang, 'Lensed water core optical fiber with potential to be used as graphene-based devices for photonic applications', Paper ID No: P03, The 3rd international conference on Optofluidics, 15-17, August, Hong Kong, 2013.

3. Y. H. Tsang, H. Long, L. L. Tao, B. Zhou, **C. Y. Tang**, "The potential of using two-dimensional materials for optical limiting applications", International conference on optical, optoelectronic and photonic materials and applications, August 2014 in Leeds, UK. (**Invited talk**)

4. Y. H. Tsang, H. Long, L. Tao, Y. Chai, **C. Y. Tang**, L. H. Zeng, "Preliminary study of nonlinear optical response of few-layer WS_2", International Conference on Small Science, December 8-11, Hong Kong, 2014. (**Invited talk**)

5. H. Long, L. Tao, **C. Y. Tang**, L. H. Zeng, Y. H. Tsang, "Layer-dependent nonlinear optical response of WS_2 nanosheet", European Materials Research Society (E-MRS 2015 Spring Meeting), May 11-15, lille Grand

Palais, France. (Oral)

6. L. Zeng, L. Tao, **C. Y. Tang**, H. Long, and S. P. Lau, Y. H. Tsang, "High-performance WS_2 nano-film photodetector", The 18th Conference of The physical society of Hong Kong, 13 June 2015. (**Invited talk**)

Acknowledgements

I would like to express my gratitude to my chief supervisor **Dr. Y. H. Tsang** and co-supervisor **Dr. C. L. Mak**, for their excellent guidance and constant encouragement throughout the period of my MPhil. study. Their high requirement, profound academic insight, and inspired discussions greatly contribute to improve the quality of my master degree research project.

I would also like to thank Prof. S. F. Yu and Dr. X. M. Zhang for their assistance on my master research.

I appreciate Dr. Ling Zhang from Laboratory of All-Solid-State Light Sources, Institute of Semiconductors, Chinese Academy of Sciences, Beijing a lot for her helpful discussions and encouragement on my research.

I would like to give my sincere thanks to my research group members, Mr. G. X. Bai, Ms. H. Long, Dr. Lili Tao for their great help in my experiments.

Finally, I would like to thank my parents for their support on my research study and life.

Table of contents

LIST OF FIGURE CAPTIONS

CHAPTER 1
Introduction

1.1 Objective

Novel laser photonic devices are a very hot and popular research topic globally as it will have a great impact on various fields including, scientific research technology development, health care industry, manufacturing industry, and military industry. My MPhil. study mainly focuses on the development of lensed liquid fiber and fabrication technology of novel carbon-based saturable absorber, which is a critical component that converts some low-cost CW laser system into high-end mode locking laser system. Mode mocking ultrafast laser is one of the most important inventions in human history, which significantly contributed to the development of different aspects of technologies, such as communication, industrial processing, and even military weapons. Thus, the research on mode locking ultrafast laser system development or corresponding applications always is the popular topic within the scientific world. In this thesis, development of novel materials and devices that can potentially be integrated into the laser photonic system throughout my MPhil. study is reported. Since some of my MPhil. research has been published in some journals and therefore part of the thesis will be identical to some of my published journal papers.

1.2 Thesis organization

Chapter 1 briefly introduces the thesis research focus and organization. In Chapter 2, the research work related to lensed liquid core fiber with controllable focusing power is presented. In Chapter 3, the research works related to carbon based saturable absorber fabrication and the ultrafast mode locking laser performance by using the fabricated absorbers within the passively mode-locked Nd: YVO4 and Yb fiber laser systems. Chapter 4 shows the conclusion of the thesis.

CHAPTER 2

Lensed liquid-core optical fiber

2.1 Introduction

Optical fiber can effectively guide light signal through an extremely long distance with very little optical loss, which makes the optical fiber a practical transmission channel for optical communication system. Owing to the favorable natures of optical fiber, such as long interaction length and huge surface area to volume ratio, the application of optical fiber not only be restricted to optical communication but also extended to another area, for examples, sensor [1], fiber laser [2] and supercontinuum generation [3-4] etc.

Typical fiber optics structure has a solid core made up of silica or plastic with a refractive index greater than that of the cladding material. In liquid core fiber, the fiber used has a hollow core filled with optically transparent fluid with low optical loss. This liquid core fiber actually facilitates lots of sensing applications. In these cases, the inspected species e.g. blood cell, glucose, nano or sub-nano particles are introduced in the liquid solvent within the hollow fiber core for further optical analysis [5-6].

As the light signal needs to be coupled into the liquid core fiber, an efficient

coupling technology is an important technique for the sensitivity of the biomedical sensor. Typically, bulky optical components, such as achromatic doublet collimator, focusing microscopic lens and precise optical stages, are used for coupling the light signal into the fiber core. These traditional coupling methods and tools are inflexible and expensive, especially when the light signal consists of different wavelength components. Another approach is to connect the liquid core fiber with a silica lensed fiber that is fabricated by mechanically polishing or thermal molding method [7-11] to form a curved end and act as a focusing lens. But obviously, the flexibility of this approach is still not sufficient for those applications which require tunable focus length of the fiber e.g. imaging application. Thus, we proposed a simple and effective technique for fabricating lensed liquid core fiber with controllable focusing power.

As briefly discussed in the introduction part, a lens that has adjustable focus by the electric field can be used as an active optical modulator. If it is inserted within the laser cavity it can potentially be used as active Q-switcher to modulate the intracavity optical losses.

2.2 Basic theory

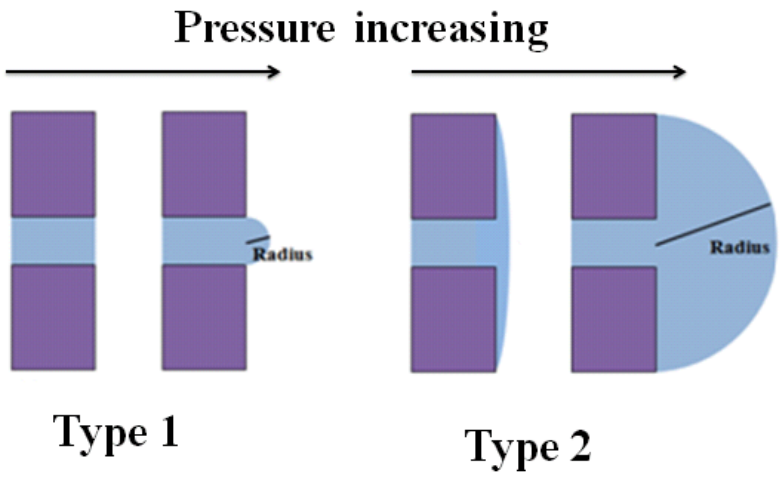

Figure 2.1 The schematic diagram shows the two geometric forms of the liquid lensed optical fiber (The purple part representing the cladding, and the blue part representing the liquid core).

For our proposed method, it is using the core liquid itself to form a curved surface and act as a focusing lens, which the core liquid is drawn out from the fiber end and form a Plano-convex lens structure as shown in Fig 2.1. Since the core liquid has certain surface tension value, the curved surface of the liquid lens is smooth and can be even better than the commercial polished solid lens. Moreover, the focusing power of the liquid lens is proportional to the radius of curvature of the curved surface, which relate to the volume of the liquid lens. The drawn flux act on the liquid lens can either come from mechanical liquid pressure or electrostatics force, which will further discuss as follow.

Theoretically, there are two cases of the liquid lens as shown in Fig. 2.1, which the aperture of the liquid lens can either be limited by the core or the cladding

diameter of the optical fiber. And it depends on the surface tension of the core liquid and the surface energy of the cladding material. If the core liquid possesses with low surface tension or the cladding material possess with high surface energy, that the aperture of the liquid lens can only be limited by the cladding since the core liquid can easily be spread over the cladding surface. Vice versa, if the core liquid possesses with high surface tension or the cladding material is low surface energy in nature, the aperture of the liquid lens will be limited by the core with a smaller radius of curvature. As the volume of liquid lens gradually increased, eventually, the liquid lens will become hemispherical in shape with a radius of curvature equal to the radius of the fiber core. If the volume of the liquid lens rises beyond the hemispherical limit, the core liquid will then spread over the cladding surface and form a liquid lens with aperture limited by the cladding diameter.

For the effective focal length *f* of the liquid lens can be calculated by three main parameters, which are *h, V* and n_{liquid}, the thickness of the liquid lens, the volume and the refractive index of core liquid. The equation can be expressed as,

$$f = \frac{1}{n_{liquid}-1}\left(\frac{h}{3} + \frac{V}{\pi h^2}\right) \qquad (2.1)$$

2.3 Variable focusing power controlled by applying water pressure

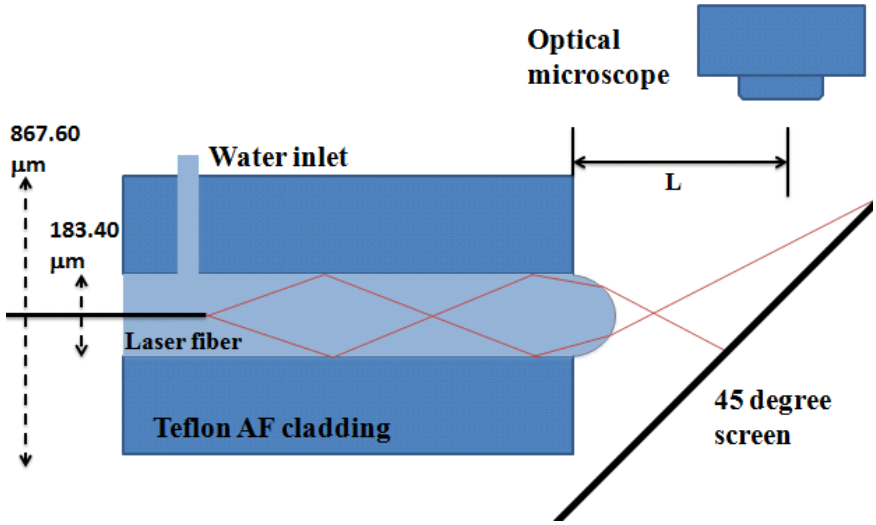

Figure. 2.2 The working principle of the Teflon-AF lensed water-core optical fiber with controllable focusing power (controlled by water pressure).

By applying liquid pressure to the liquid inlet, it can control the volume of the formed liquid lens and vary the focal length of the lensed liquid core optical fiber. Deionized water (light water) is selected as the core fluid and company with Teflon AF polymers as the cladding material.

Lots of biomedical substance and nano-particle can be easily introduced into the water. It makes the research on water core fiber important for the biomedical application. Besides, water also has a great nonlinear refractive index of 1.60×10^{-16} cm^2/W [4], low optical loss in UV wavelength range [6] and almost zero dispersion on 1060 nm wavelength [12], which also implies the water core optical fiber can be used as an optical waveguide to delivery UV and near 1

micron CW or pulsed laser.

For the Teflon-AF hollow fiber, it has several advantages, including high optical clarity, good mechanical strength and chemical resistance. More importantly, it possesses the lowest refractive index of any known transparent polymer, 1.290. Therefore, Teflon-AF is the one of the very few solid state materials that has a refractive index lower than water, 1.330 and suitable to be used as the cladding of the water core optical fiber.

For the experimental setup, the Teflon AF hollow fiber was filled with deionized water through the water inlet as shown in Fig 2.2. The core and cladding diameter of the hollow Teflon AF fiber are 183.40 μm and 867.60 μm, respectively. And the numerical aperture is 0.324 as deionized water was used as the core liquid. The detailed experimental results for the tunable lensed optical fiber controlled by mechanical liquid pressure is reported in my previous publication [13]. However, the tuning speed of the lens focal length is relatively slow and the focal length of the lens cannot be controlled precisesly. Additionally, parabolic shape tip lens cannot be produced by this method.

2.4 Variable focusing power controlled by applying electrostatic force

In this chapter, a unique method to fabricate liquid-core lensed fibers by filling water into hollow Teflon AF fiber was demonstrated. The radius of curvature of the liquid lens can be controlled by adjusting the applied voltage on the fiber core so as to produce parabolic shaped lens with enough applied voltage.

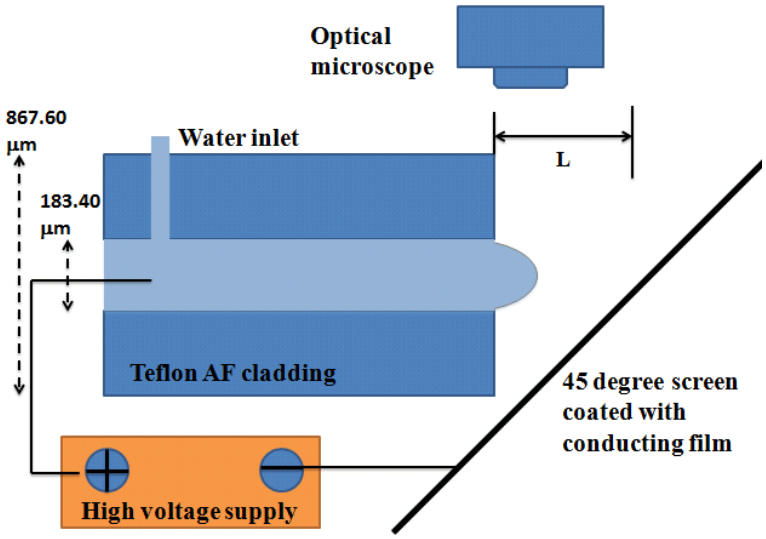

Figure 2.3 Schematic diagram of the experimental set-up to produce variable focal length of the lensed liquid core fiber under the strong electrical field created at the fiber tip.

As shown in Fig. 2.3, the setup of the liquid core lensed fiber is similar to Fig. 2.2 excepting a high voltage is applied across the core liquid and the 45 degrees titled screen in order to generate a strong electric field between them. As the voltage applied, the core liquid is positively charged, which each of the liquid

molecules will repulse to each other, thus it will generate a driving flux to push the core liquid out of the fiber end and formed the liquid lens. Besides, the negative charged conducting surface on the 45-degree screen will also attract the liquid lens toward it. By the Tip-plane model [14-15], it can express the generated electric field as follow,

$$E(X) = \frac{L \cdot V}{X(2L - X) + (L - X)r} \cdot \frac{1}{In[2(L/r)^{1/2}]} \qquad (2.2)$$

where V is the applied voltage, L is the distance between the fiber tip and the conductor plane, r represents the radius of the fiber core or the cladding depending on the lens limited by either the core diameter or cladding diameter. X is the distance from the fiber tip to the calculated position. With the formation of the E-field at the apex of the liquid lens, electro-osmosis flow occurs and carries the core liquid toward the apex of the lens [16]. Nevertheless, a pressure field is induced to balance the osmosis flow. The result net flow v is,

$$v = -(\frac{\varepsilon E\varphi}{\eta}) - (\frac{h^2}{3\eta})\nabla p \qquad (2.3)$$

where ε and η are the dielectric constant and viscosity of the core liquid, respectively. ϕ and h are the surface potential and the maximum thickness of liquid lens, respectively. In equilibrium, the net flow v is equal to zero and the applied voltage V(x,y) is proportional to the induced pressure p(x,y) by

$$-\varepsilon\phi V(x,y) = 1/3(\mathrm{h}^2\ p(x,y)) \qquad (2.4)$$

The induce pressure field is inversely proportional to radius of curvature of the lens R by p =2γ /R, where γ is the liquid surface tension and further on,

$$1/R = 3/2(\varepsilon\phi/\gamma \cdot h^2)V(x,\mathrm{y}) \qquad (2.5)$$

These equations indicate a decrease in the radius of curvature of the liquid lens with the increase of the applied voltage. In this experiment, hollow Teflon AF fiber and deionized water core fluid were used to construct the liquid core fiber. A RS silver loaded electronic conducting film was coated on the (5 x 10 mm) 45 degrees titled stainless steel plate by spin coating method and the plate is connected to the high voltage supply. A 100 μm diameter copper wire is inserted through the liquid inlet in order to generate a positive charge in the core liquid. The initial distance between the fiber tip and the conducting plate was 2 mm, the applied voltage is then gradually increased and the transformation of the water lens is observed by the optical microscope. The method of using electrostatic driving force to control the liquid lens is available for both case of aperture limited by either core or cladding diameter as shown in Fig. 2.4 & 2. 5.

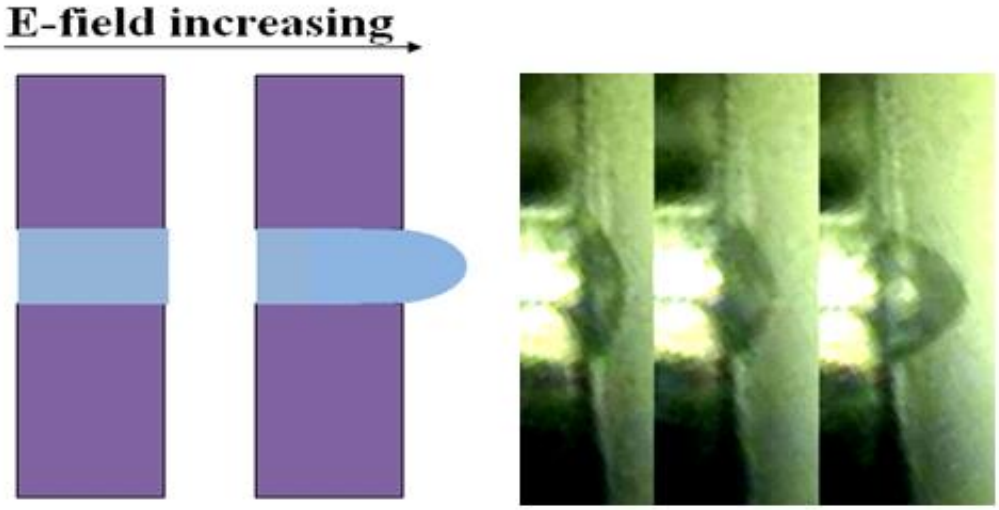

Figure 2.4 The schematic diagram and image captured by an optical microscope to show the transformation of the water lenses with respect to the rising applied voltage which the aperture is limited by the Teflon AF fiber core diameter.

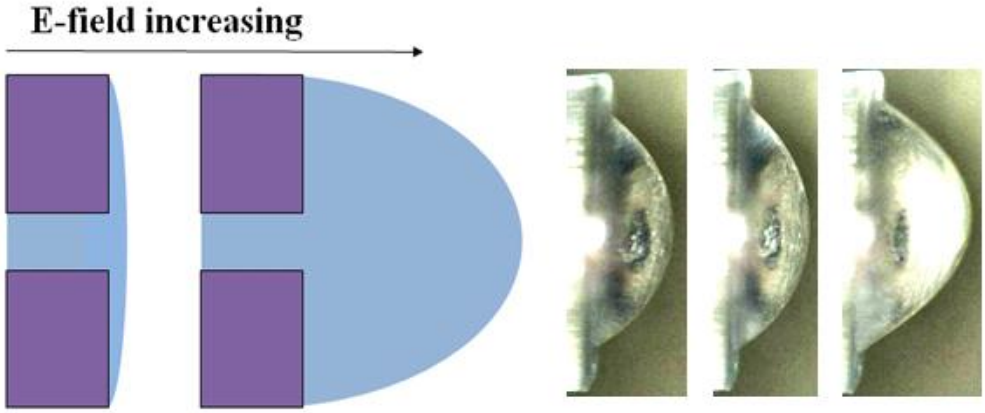

Figure 2.5 The schematic diagram and image captured by an optical microscope to show the transformation of the water lenses with respect to the rising applied voltage which the aperture is limited by the Teflon AF fiber cladding diameter.

As shown in Fig. 2.4 & 2.5, the water lens is first to act as spherical shape lens as the applied voltage is low, but upon the voltage increased to a sufficiently high

level, that the lens will eventually transform into parabolic shape. The lens shape with respect to different voltages is shown in Fig. 2.6. Before the voltage applied, the core water is slightly pumped out from the fiber end to form a water lens with a relatively large radius of curvature in this case the aperture is limited by the core diameter. As the voltage applied increased, the volume of the water lens is rising and the radius of curvature of the lens decreases gradually. When the applied voltage reached 2.6 kV, the water lens becomes hemispherical in shape with the radius of curvature close to the radius of the Teflon fiber core. In the spherical lens shape range, it can show that the radius of curvature of the lens is in a linear relationship with the applied voltage as refer to Eq. 2.5.

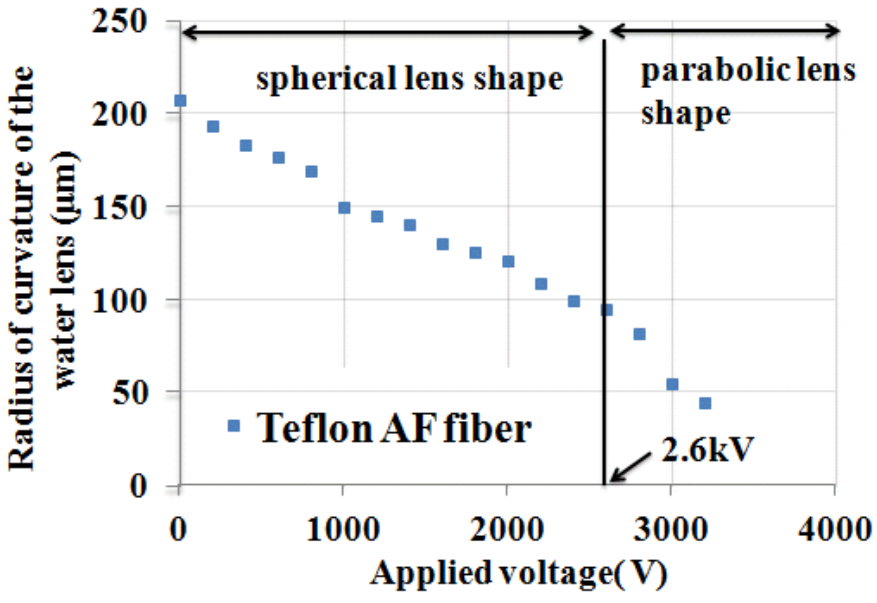

Figure 2.6 To show the experimental results of the radius of curvature of the water lens according to the rising applied voltage(distance between the fiber tip and conducting plane L =2mm).

As the applied voltage further increased, the shape of the water lens started to transform into a parabolic lens shape. But upon the applied voltage reached around 3.2 kV, Taylor cone formed as shown in Fig. 2.7, which also can be observed during electro-spinning process. The focal length of the water lens varied from 0.628 mm to 0.111 mm with respect to the change of applied voltage from 0 V to 3 kV (L =2mm).

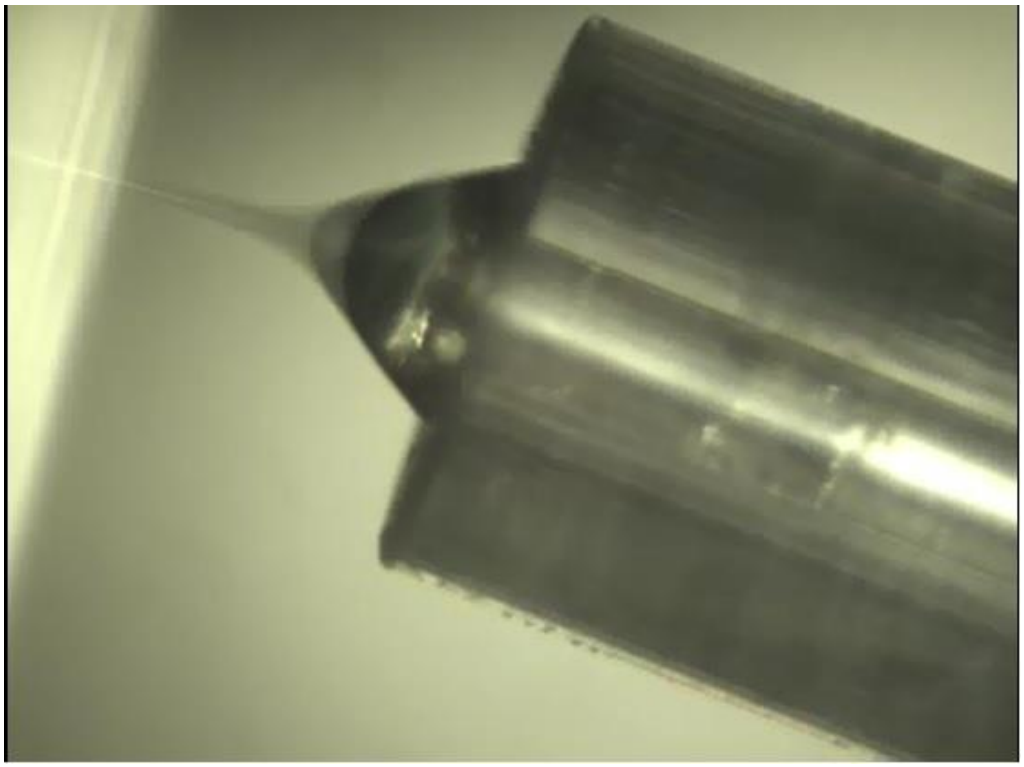

Figure 2.7 The Taylor cone formed when the applied voltage reaches beyond 3.2 kV.

2.5 Summary

In this study, it has demonstrated a unique method to fabricate liquid-core lensed fibers with controllable lens shape (semi-spherical / parabolic) and radius of curvature of the lens by adjusting the applied voltage. The experiment has successfully demonstrated a variation of focal length from 0.628mm to 0.111mm responding to the change of applied voltage from 0V to 3 kV (L = 2mm) for the Teflon AF fiber (water core dia. 183.4 μm, Teflon cladding dia. 867.6 μm, NA = 0.324). Further increase the applied voltage into 3kV, the shape of the liquid lens will start to transform into Taylor cone. Further works can be done to solve the liquid evaporation problem of the liquid lens by adding a elastic film on top of the liquid lens. Besides, the work of integrating this lensed fiber into laser system to modulate optical loss within the laser cavity is still continuously processing.

CHAPTER 3

Carbon based saturable absorber fabrication and diode pumped solid state mode locked laser

3.1 Introduction

3.1.1 Ultrafast laser features and its applications

Laser processing is one of the most advanced and effective method employed in various fields including industrial, medical and scientific research. Industrial applications, for example, laser welding [17-18], cutting [19] and hardening [20] are already well developed in the past two decades. The laser processing quality and precision of typical CW or long pulse high power laser sources are not sufficient enough for some modern high technology applications such as silicon wafer cutting or surface processing for integration circuit fabrication [21] and sapphire wafer processing [22] for cutting the screen of the smartphone or LED substrate. The traditional "hot ablation" will lead to the rough edge and induce heavy damage to the surrounding materials due to the thermal energy diffusion as corresponding to the long laser pulse duration as shown in Fig. 3.1. As the heat transfer velocity in the common material is about few nanosecond [23], if the laser pulse duration is greater than the heat diffusing velocity such as Q-switching solid state laser with a pulse width greater than 10 ns, the heat will transfer from the irradiated area to the surrounding and enlarge melting zone. Besides, the non-uniform melting velocity will lead to unsharp cutting or rough edge as shown in Fig. 3.2. Vice versa, if the pulse width is in the

picosecond or femtosecond region (much shorter than the heat diffusing velocity), the produced pulse peak power will become extremely large compared with the laser operating at CW or ns Q-switched mode. In this case, due to the ultra-short interaction time, the irradiated area of the processing material will be vaporized instantaneously by the extremely high peak power and there is not enough time for heat transfer to enlarge the affected zone [24]. Thus, the ultrafast laser processing is also called “cold ablation” and produces smooth cutting edge.

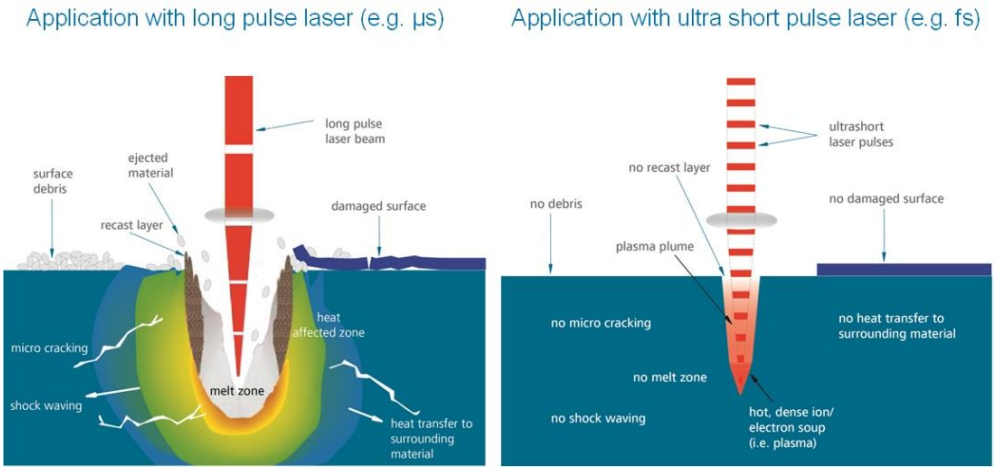

Figure 3.1. The comparison of the material processing result which using CW or long pulse laser source and ultrafast short pulse laser source. [25]

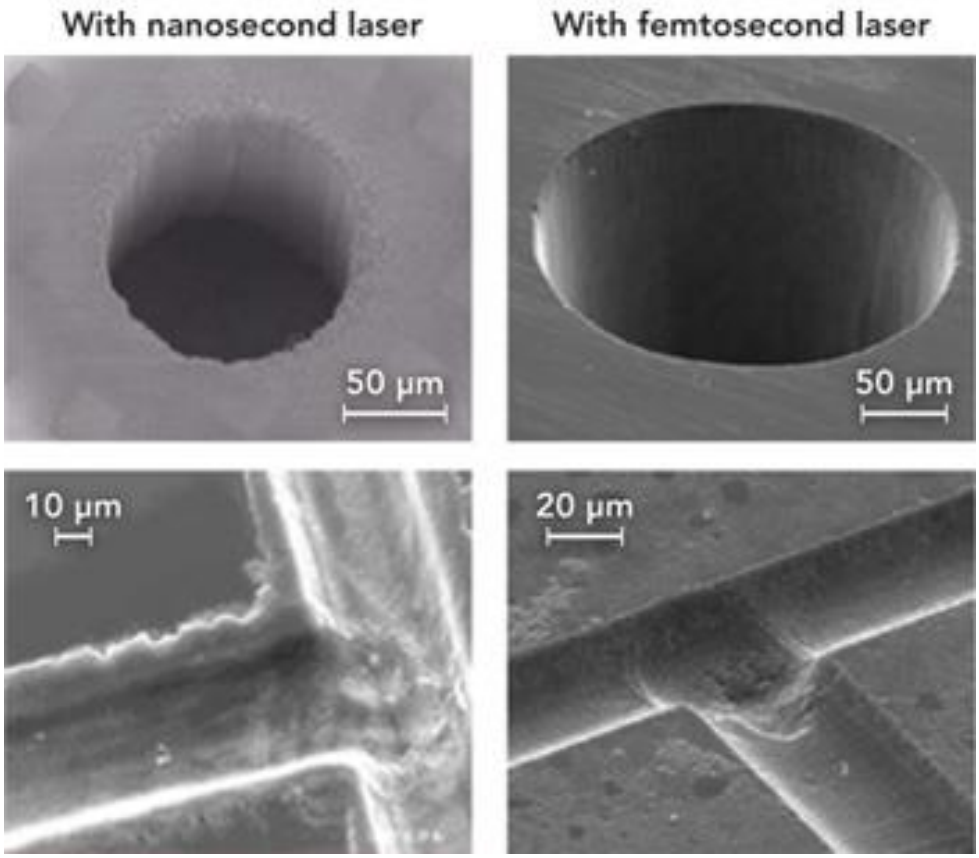

Figure 3.2 Laser processing on glass with a 266 nm (UV) ns-laser (left-side) and with a 780 nm 100-fs laser (right-side). [26]

Due to the multi-photons absorption occurs under ultra-high pulse peak power, the ultrafast laser is able to process almost any kind of materials, including transparent materials [27-28]. For example, the picoseconds or femtoseconds laser is very useful for cutting sapphire wafer. On the other hand, the ultrafast laser is also popular for the biomedical application, such as nanosurgery [29], Photodynamic therapy, PDT, which is a method to selectively eradicate malignant cells while leaving the normal cells intact [30-31]. For the biomedical applications, able to control the energy deposition is a critical issue as even a small rise in temperature within the living cell may kill it. The ultrafast laser can

provide a precise energy delivery mechanism to achieve clear-cut with very little damage to the surrounding tissue. Therefore, the study and development of the ultrafast laser always attract great interests for both industrial and scientific research. In this chapter, we are focusing on the design and fabrication of ultrafast seed laser source by using some novel materials and techniques.

3.1.2 Theory of mode locking laser

For the generation of the picoseconds or even femtosecond ultrafast laser pulse, it typically achieved by mode locking technology [32-35]. Within the laser system, the bandwidth of operation is gain medium dependent. The bandwidth of generated frequencies is governed by the gain bandwidth of the laser gain medium. For example, Titanium-doped Sapphire (Ti:sapphire) solid-state laser has a gain bandwidth of around 128 THz leads to produce wavelength bandwidth of 300 nm centered around 800 nm [36]. The another parameter which able to effectively affect the emission frequencies of the laser system is the optical cavity length.

Only the laser frequency obtained the boundary condition set-up by the two cavity mirrors can be built up within the laser cavity. These discrete set of

frequencies is called the longitudinal modes of the laser cavity. For a simple plane-mirrors cavity, the produced longitudinal mode wavelengths λ is given by Eq. 3.1,

$$L = \frac{n\lambda}{2} \qquad (3.1)$$

where *n* is an integer which defined as the mode order and L is the cavity length. Typically, *L* is much larger than *λ*, so the relevant values of *n* are great, such as around 10^5 to 10^6. And the frequency separation between any two adjacent modes *n* and *n*+1 is defined as Δν and shown in Eq. 3.2

$$\Delta\nu = \frac{c}{2L} \qquad (3.2)$$

where *c* is the speed of light. By Eq. 3.2, laser with a mirror separation of 0.3 meters has a frequency separation between longitudinal modes of 0.5 GHz.

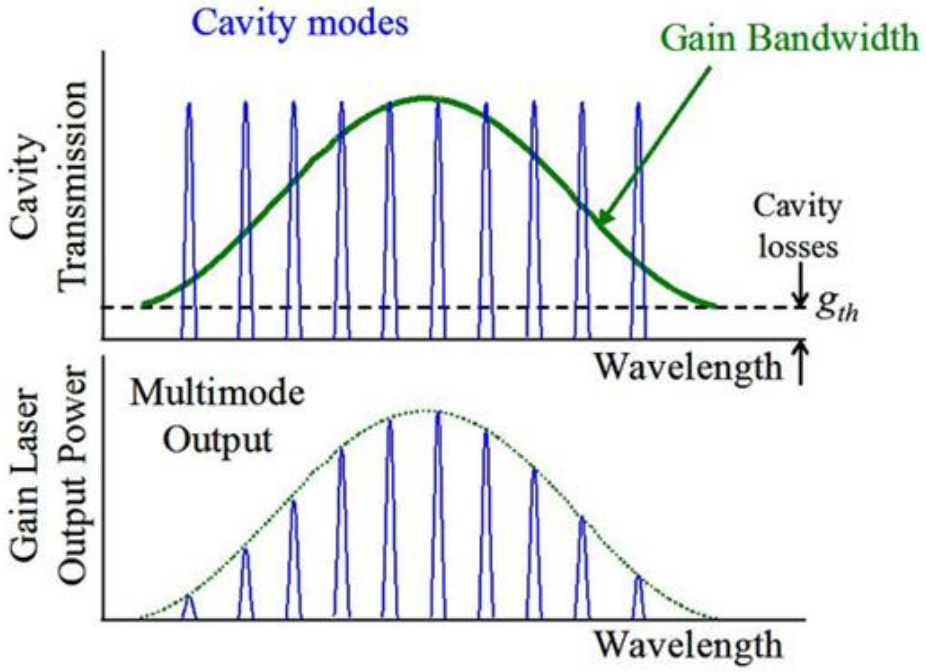

Figure 3.3 Cavity resonance modes and gain bandwidth.[37]

As shown in Fig 3.3, by combing the gain bandwidth, the allowed cavity mode is enclosed within the gain bandwidth envelope. Thus for a Ti:sapphire laser with 128 THz gain bandwidth and 3 meters cavity length is able to support almost 256,000 modes. Each individual longitudinal mode has a certain narrow range of frequencies over which it operates, but typically this bandwidth, affected by the Q factor of the cavity is much less than the intermode frequency separation. Each of the individual longitudinal modes is oscillating independently. Besides, there is no fixed phase relationship between each mode, instead, it varies randomly due to the thermal fluctuation in the laser system. For lasers with just several oscillating modes, the interference between these modes can lead to beating effects in the laser output, which cause output intensity fluctuations. If the lasers system has thousands or even greater mode number, the interference effects will tend to average out and produce stable output intensity, which is also known as Continuous Wave (CW) laser. Furthermore, if the individual mode operates with a fixed phase corresponding to each other, different from CW laser output, these modes will periodically all constructively interfere with each other and generate a pulse with ultrashort duration and high peak power intensity. And this phenomenon is known as mode-locking. The mode-locked pulses occur separated in time by

$$\tau = \frac{1}{\Delta\nu} = \frac{2L}{c} \qquad (3.3)$$

which τ is the time taken for the light to travel through exactly one round trip of the laser cavity, thus τ was also known as round trip cavity time. The produced pulse train with repetition rate agree well with the round trip cavity time is evident for successful mode locking. Besides, the duration of each pulse is determined by the number of modes that are oscillating in phase, but in the real case, not all of the laser modes will be phase-locked. If there are N modes locked with a frequency separation Δν, the overall mode-locked bandwidth is NΔν. The broader the mode-locked bandwidth leads to the narrower laser pulse duration. Additionally, the pulse duration is affected by the pulse shape, in other words, it is determined by the exact amplitude and phase relationship of each longitudinal mode. For example, for mode-locked pulses with a Gaussian temporal shape, the minimum possible pulse duration Δt is given by

$$\Delta t = \frac{0.441}{N\Delta\nu} \qquad (3.4)$$

The value 0.441 is defined as the 'time-bandwidth product' and it is depending on the pulse shape. For the Ti:sapphire laser, the minimum possible pulse duration achieved is around 3 femtoseconds [38-39]. This value represents the shortest possible pulse duration can be achieved. In practical case of a mode-locked laser, the actual pulse duration will be affected by different factors including the actual

pulse shape and the overall dispersion of the cavity.

3.1.3 Active mode locking

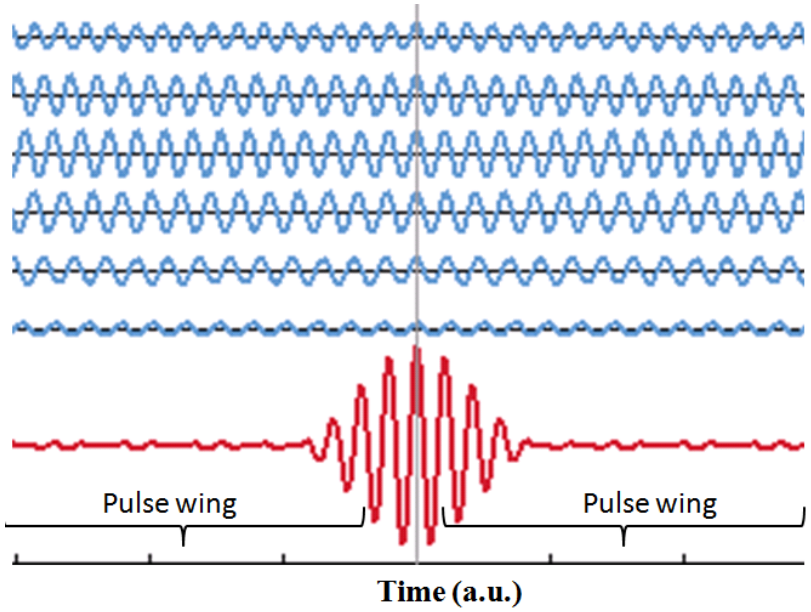

Figure 3.4: Interference simulation result of the 7 different longitudinal modes with a slightly different frequency pulses oscillating within a laser cavity.[40]

As discuss previously, by the interference of the longitudinal modes within the laser cavity, there is beat effect occur. Nevertheless, as the modes are not phase-locked with each other continuously, the output will be balanced by the random fluctuation of modes within the cavity eventually and act as a CW output. However if there is a mechanism inhibited the pulse wing in the beat condition and only allow the center intense pulse peak be amplified and oscillated in the cavity repeatedly, a pulse train with ultrashort pulse duration could be generated. To achieve this, the optical loss within the laser cavity can be actively modulated with frequency synchronized with the resonator round trip cavity time, which is

known as active mode-locking. The active mode-locking effect can effectively eliminate the pulse wing and eventually shorten the pulse duration of the mode-locked pulse as shown in Fig 3.4 & 3.5. Typically, active mode-locking can be achieved by inserting either acoustic-optic [41] or electro-optic modulator [42] within the laser cavity. Another mechanism for modulating optical loss with high speed can also be used to achieve active mode locking. A popular choice to achieve active mode locking is Pockels cells, which an electrical signal is used to modulate the transmission ratio, refractive index or polarization state of the cell to modulate intracavity optical loss.

However, active mode locking usually is more expensive as it requires more complicated design, expensive driver, and signal generation. Besides, the modulating signal needs to be precisely controlled to match the round trip cavity time in order to achieve stable mode lock pulse operation. This calibration process is known as synchronization and it further increases the complexity of the laser system. Furthermore, as the relaxation time of the active mode locker is relatively long, such as in nanosecond range, it will also affect the pulse width shortening process and result in long pulse duration. These are the disadvantages compared with the passive mode locking.

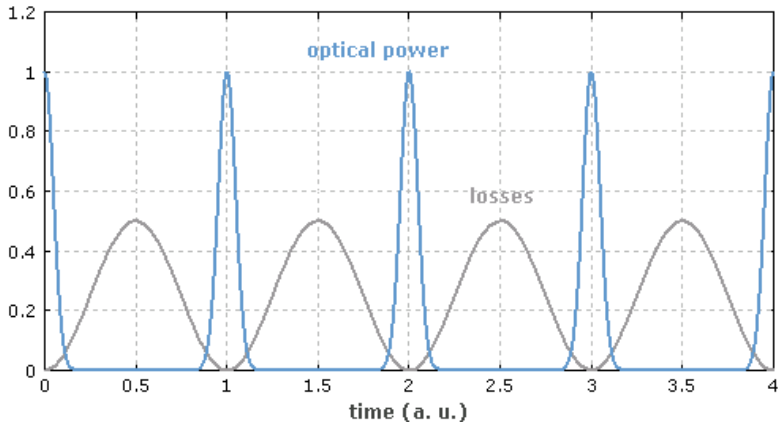

Figure 3.5 Schematic diagram shows the mechanism of active mode locking, which optical loss within the cavity is relatively large corresponding to the pulse wing position. [43]

3.1.4 Passive mode locking and saturable absorber

Provided the laser modulator can operate passively and automatically adjust its own optical loss with synchronized round trip cavity time, the overall mode locking laser design can greatly simplified and reduce the production cost. This automatic variation of the optical loss is known as passive mode locking, and can be achieved by using Saturable Absorber (SA), which is an optical device with strong optical nonlinearity and capable of varying its transmission ratio based on the incident light intensity as shown in Fig 3.6.

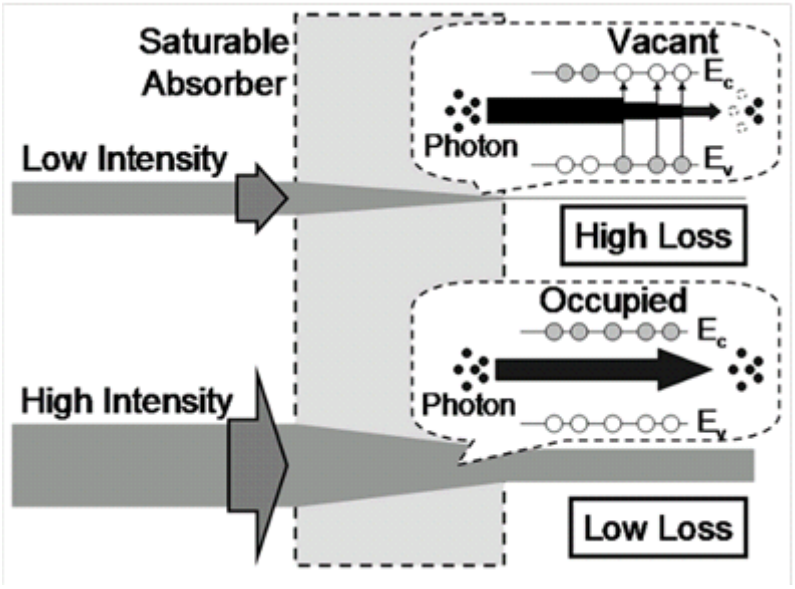

Figure 3.6 Schematic diagram shows the saturable absorption (E_v and E_c denote energy levels of the valence band and conduction band, respectively). [44]

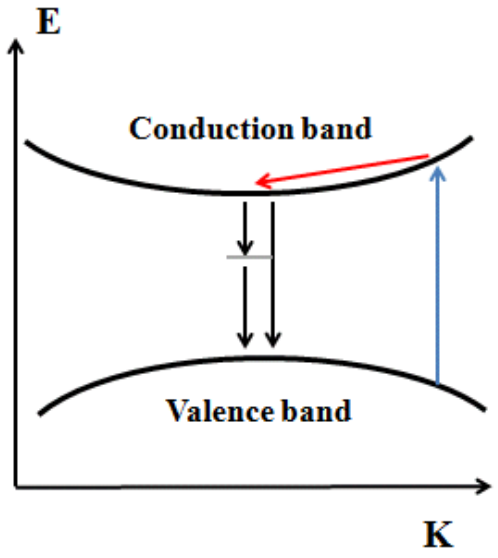

Figure 3.7 Schematic diagram shows the excitation and relaxation of carriers in a semiconductor.

As the SA is excited by a photon with an energy matched with the SA bandgap energy as shown in Fig. 3.7, the valence electron is excited to the conduction

band. Further on, there is a relatively fast thermalization relaxation within the conduction and valence band with a time scale of few tens of femtoseconds. Then it follows by the process of carriers recombine, usually acompany with some crystal defects. Under the low light intensity excitation, the electron excitation rate is smaller than the decay rate and the absorption of the SA remains unsaturated. As the incident optical intensity increases, excited electrons will accumulate in the conduction band, which causes the electrons in valence band exhausted. [24] As a result, the transmission ratio of the absorber is significantly increased (close to 100%) after it is saturated by introducing a short intense pulse, the absorption of saturable absorber will then be recovered by the intraband thermal relaxation and further on electron-hole pair recombination. Ideally, the saturable absorber will selectively absorb low-intensity light (attenuate low-intensity light - pulse wings) and transmit light with intensity high enough to saturate the absorber.

3.1.5 Ultrafast laser development

For the ultrafast laser development, in the early 70s, dye mode-locked laser takes the dominant position [45-46], which subpicosecond pulse was first demonstrated in the dye laser [47] and followed by further external compression to achieve few femtoseconds pulse output [48]. The research in Ti-sapphire mode

locking laser gain medium leads to a technology breakthrough in the late 80s. The natural gain bandwidth of Ti:sapphire is broad enough to produce femtosecond pulse without pulse compression [49]. In 1990, Kerr-lens mode locking (KLM) effect on Ti:sapphire laser was first demonstrated [50]. Kerr lens effect actually is a refractive index variation mechanism which induced by nonlinear response of a Kerr medium to the incident light. The refractive index of the Kerr crystal is affected by the incident light intensity. Assuming the incident light beam with a Gaussian shape, which the power density distribution is not uniform. In the Kerr medium, the corresponding varied refractive index is determined by the index distribution, where the index for the incident light is higher in the medium center than that on the edge. As a result, it will generate a simulated lens feature within the Kerr medium as shown in Fig 3.8, which is known as self-focusing. By using either a hard aperture to directly cut-off the intracavity laser beam to modulate the optical loss within the cavity (Fig 3.9), or a soft aperture to modulate the overlap level of pump light and the simulated laser within the cavity (Fig 3.10), the optical gain with the cavity is passively modulated and thus induce passive mode-locked short pulse. However, the Kerr lens mode locking is difficult to achieve stable operation.

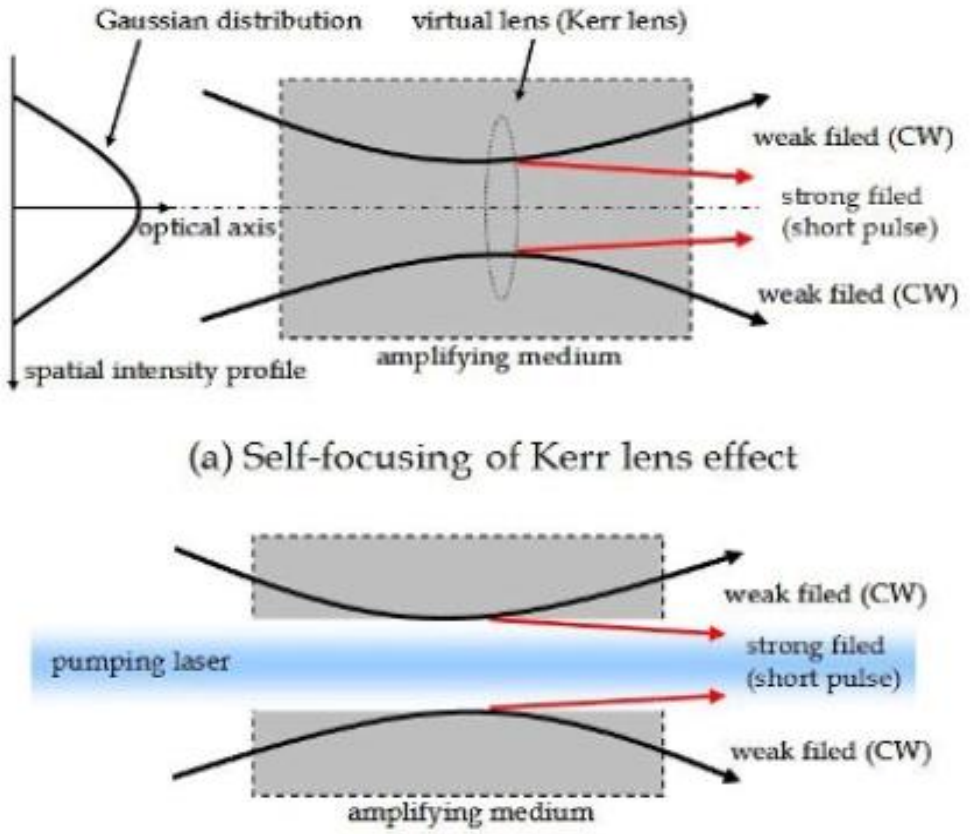

Figure 3.8 Schematic diagram of the principle of Kerr lens effect [51].

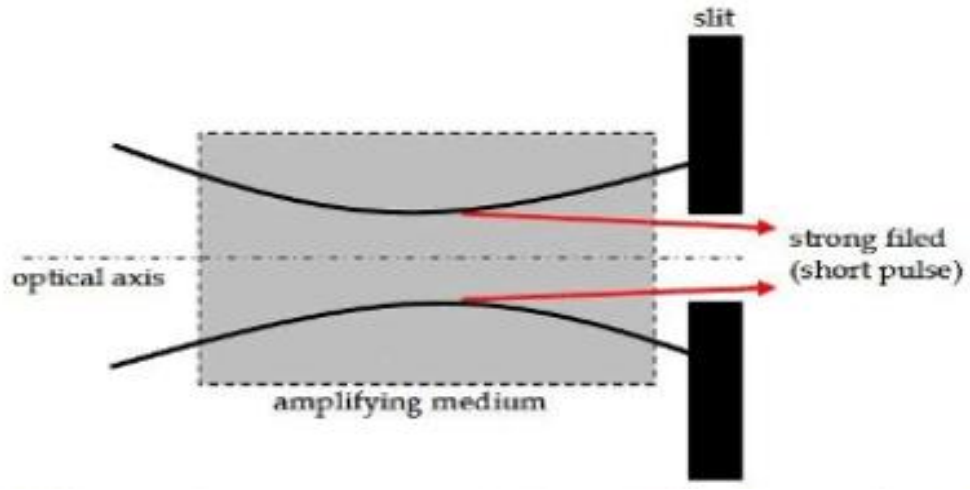

Figure 3.9 Schematic diagram of hard aperture process of Kerr-lens mode locking[51].

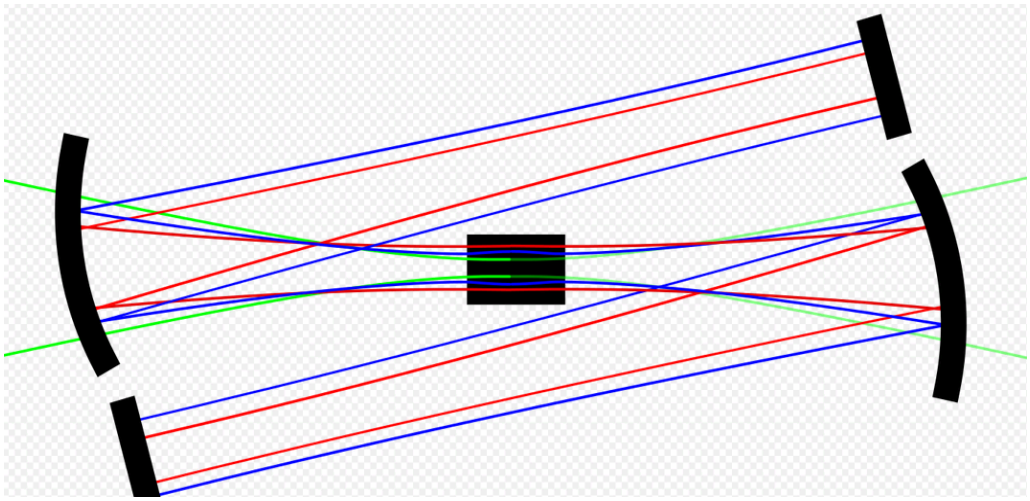

Figure 3.10 Schematic diagram of soft aperture process of Kerr-lens mode locking (Green line representing the pump beam, red and blue line representing the CW laser beam and pulsed laser beam, respectively) [52].

Semiconductor saturable absorber mirror, SESAM, is integrated into a mirror system to form a reflective type saturable absorber. Fig 3.11 shows an example of SESAM geometrical construction [53]. It composes of four layers. The bottom layer is a GaAs plate, and the second layer is a Bragg reflector formed by pair combination of GaAs and AlAs to control the reflected central wavelength. The third layer is a semiconductor saturable absorber, which is selected depending on the operation wavelength, such as InGaAs quantum well is commonly used for 1 micron operation. And the top layer is covered by a second reflector. Unlike the Kerr lens mode-locking effect, the application of the SESAM is not restricted by the cavity design, thus, it can be used for a broader range of laser cavity design.

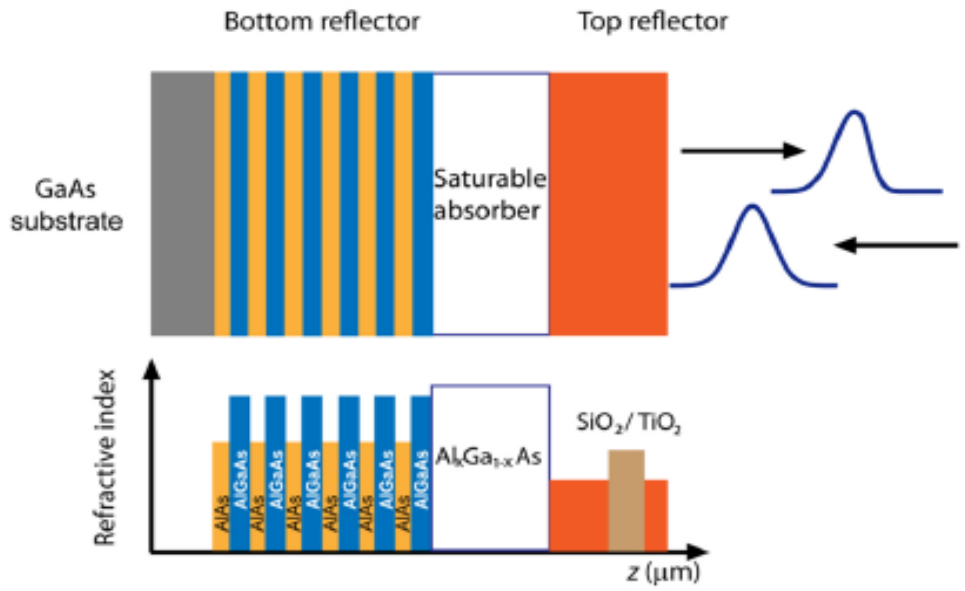

Figure 3.11 Structure of Semiconductor Saturable mirror [54]

And by the selection of the absorber layer material and precious parameter adjustments in the Metalorganic Chemical Vapour Deposition (MOCVD), the nonlinear properties of the SESAM can be effectively controlled, such as the saturable fluence or relaxation time. This feature makes SESAM practical for commerilized mode locking system.

However, the SESAM is wavelength sensitive with narrow operational waveband and require relatively expensive Metal Organic Chemical Vapor Deposition MOCVD technique [55]. Thus, development of new type material with good nonlinear saturable absorption properties and low fabrication cost are continuously attracting great research interests.

3.2 Laser cavity design and mode locking laser characterization

The experimental set-up was shown in the following figure.

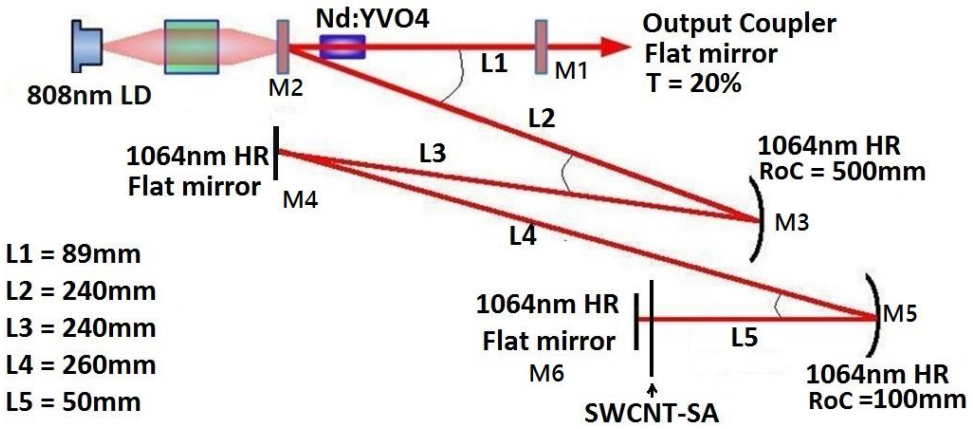

Figure 3.12 6 mirrors solid state laser system (170MHz mode).

The laser gain crystal used is Nd:YVO_4 with 0.5% Nd doping concentration and it was purchased from Castech Inc. Chian. The dimension of the a-cut Nd:YVO_4 crystal is 3 mm x 3 mm x 8 mm. In this study, the 6 mirrors used to construct the laser cavity are:

M1 mirror – flat output coupler: partially reflecting light at 1064 nm. Different coupling percentage is selected to optimize the output power.

M2 mirror: Flat mirror, High Transmission, HT, at 808 nm and High Reflection, HR, at 1064 nm, which allows 808 nm pump light transmitted into the laser cavity and launched into the laser gain medium.

M3 mirror: Concave with RoC 500 mm, HR at 1064 nm.

M4 mirror: Flat mirror HR at 1064 nm.

M5 mirror: Concave with RoC 100 mm, HR at 1064 nm.

M6 mirror: Flat, HR at 1064 nm.

M6 can be substituted by reflective type saturable absorber, e.g. SEASAM as it is integrated with HR mirror. Without any saturable absorber mode locker inserted into the laser cavity, CW mode operation will be achieved. A transmission type saturable absorber is needed to be inserted into the laser cavity at the right position in order to produce passive mode-locking pulses. The six mirrors are used to control its intra-cavity beam waist diameter and cavity length and both parameters are very important for the mode locking laser pulse formation. In order to produce stable CW mode locking pulses, the incident fluence on the saturable absorber (given in Eq. 3.5) needs to be higher than the saturable fluence of the saturable absorber.

$$\text{Incident fluence} = \frac{\text{Intra-cavity power}}{\text{Incident area on the SESAM mirror or SWCNT absorber}} \quad (3.5)$$

Therefore, it is very important to calculate the intra-cavity lasing mode radius. A MathLab computer program based on ABCD matrix is written with computer code shown in the appendix of this thesis to calculate the intra-cavity lasing mode radius. The thermal lensing effect is also needed to be considered for the cavity beam waist modeling as for the high power operation the laser crystal will be pumped with high power by the 808 nm pump source. The energy loss during the laser conversion will become heat energy and produce thermal lensing effect and the heated laser crystal will act like a thin optical lens [56-57]. This thermal lens acts like an additional concave mirror, in here it is called mirror T, MT, inserted into the laser cavity with focusing power depending on the pump power to the laser crystal. In the simulation, the thermal lensing effect is taken into consideration, which the thermal lens is considered as an additional concave mirror to account for the different between the simulated results and the real case under high pumping power. Thus in the simulation, 7 mirrors in total are used for the calculations.

The thermal lensing effect can be calculated by Eq.3.6

$$\frac{1}{f} = \frac{\left(\frac{dn}{dt}\right)}{2\varkappa A} P_{heat} \qquad (3.6)$$

where P_{heat} is the dissipated power, A is the pumped area, κ and $\frac{dn}{dt}$ are the thermal conductivity and thermo-optic coefficient of the gain medium. The

thermo-optic coefficient dn/dT of Nd:YVO_4 is 2.9e-^{6} /K and the corresponding thermal conductivity κ of Nd:YVO_4 is 5.1 W/(m K).

The higher the pump power, the greater is the thermal lensing effect and lead to the smaller radius of curvature of MT. The simulated results are presented in Fig 3.13 and Fig 3.14.

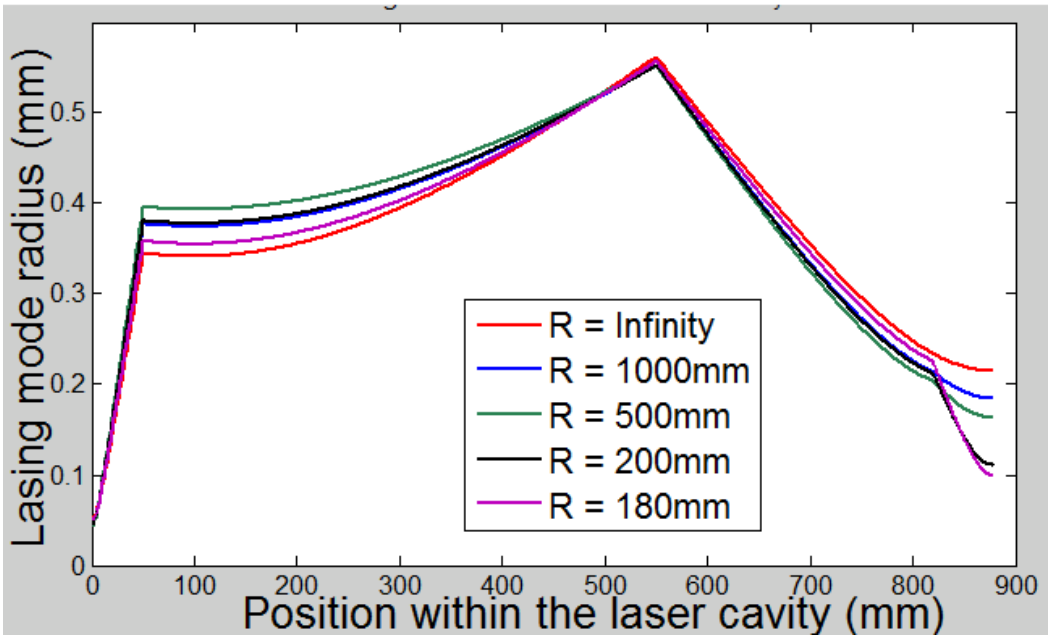

Figure 3.13 The simulated radius of 1064nm lasing mode inside the laser cavity under different level of thermal lensing effect (170MHz mode). R - Radius of Curvature of MT

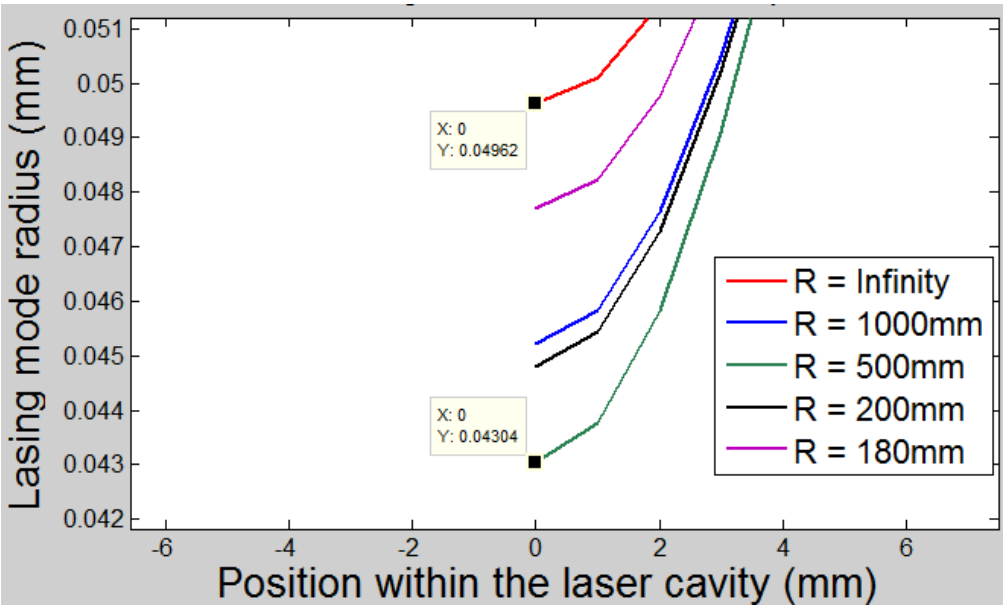

Figure 3.14 The simulated radius of 1064 nm lasing mode inside the laser cavity under a different level of thermal lensing effect (The intra-cavity beam waist is on the front surface of the end laser mirror). R - Radius of Curvature of MT

As shown in Fig. 3.13, the thermal lensing effect can affect 1064 nm lasing mode radius within the cavity greatly. The different R-value stands for the radius of curvature of MT, R equal to infinity mean there is no thermal lensing. In this case, the R = 180 mm is the threshold value. For R < 180 mm, the cavity will become not stable.

Base on the simulation shown in Fig 3.14, the intracavity beam waist is on the front surface of the M6 and it is depending on the thermal lensing effect as well. If the thermal lens radius decrease, the radius of the beam waist will also reduces. For example, the radius of the lasing modes are 49 μm and 43 μm mm with respect to R = infinity and 500 mm, respectively. This model confirmed the

thermal lensing effect can potentially increase the optical incident fluence on the saturable absorber and it may reduces the mode locking pulses stability and degrade overall performance of the mode locking laser system by damaging the reflector or saturable absorber. This simulation allows us to check out the stability of the laser cavity and estimate the incident fluence on the saturable absorber. We can compare the intracavity incident fluence to the saturable fluence of the absorber to evaluate the possibility to achieve mode locking operation at certain pumping power.

The intracavity beam waist is set on the front surface of the end mirror in order to achieve maximum laser incident fluence on a reflective type saturable absorber replacing M6 in order to obtain a the passive mode locking operation

Mode locking laser characterization

The repetition rate of the mode locking laser pulses is determined by the round trip cavity time. Each generated laser pulses will travel around the cavity from the output coupler before the another laser pulses can be coupled out from the output coupler.

$$\text{Round trip cavity Time} = \frac{2 \text{ x Total cavity length}}{\text{Speed of light}} \qquad (3.7)$$

$$\text{Repetition rate of the pulse signal} = \frac{1}{\text{Round trip cavity Time}} \quad (3.8)$$

The repetition rate of the laser pulses generated can be characterized by the photodetector shown in Fig. 3.15 and a high speed digital oscilloscope (shown in Fig.3.16).

Figure 3.15 Thorlab DET10A High-speed photodetector with 1ns rise time.

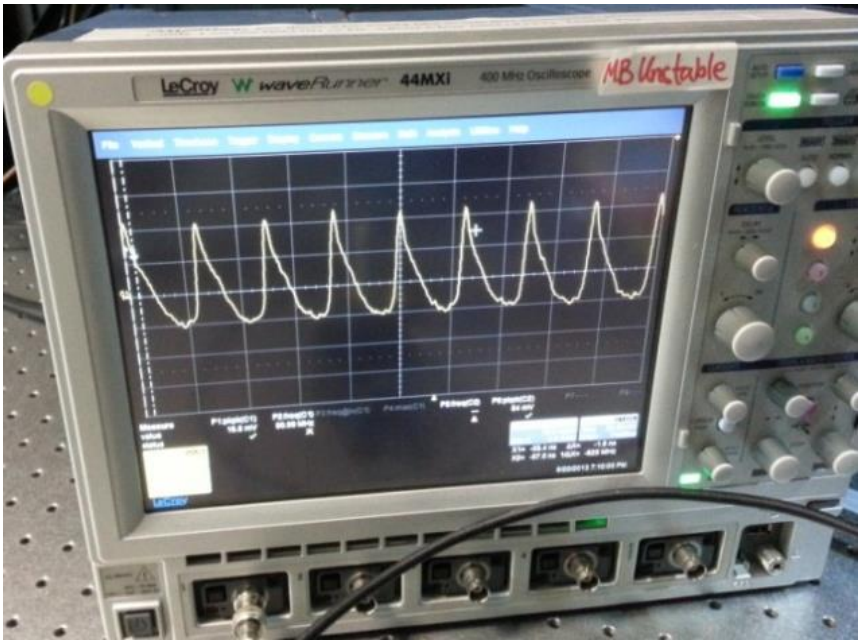

Figure 3.16 Lecroy oscilloscope Waverunner 44MXi (5GSa/sec, 400MHz Digital Oscilloscope).

By observing whether the repetition rate of the output laser pulse train matches with the round trip cavity time calculated by Eq. 3.7 & 3.8. We can confirm if the passive mode-locking pulses are successfully achieved. Generally, the laser mode locking pulses width is very short in the region of ps and fs. Therefore an autocorrelator, Femtochrome FR-103XL as shown in Fig. 3.17 is used to measure the pulse duration of the mode locking laser.

Figure 3.17 Femtochrome FR-103XL Autocorrelator.

3.3 SWCNT saturable absorber fabrication

Typically, reflective or transmission type SWCNT absorber is fabricated by spin coating [59], spray coating, vertical evaporation coating methods [58-59]. However, it is difficult to ensure uniform deposition of CNT over a large area via spin or spray coating methods. Vertical evaporation method has disadvantages such as long fabrication time, raw material waste and so on. Dip coating proposed in this study is a mainstream technique for industrial fabrication of large area film materials. High-quality film with large surface area, controlled thickness, good uniformity and continuity can be produced by this proposed dip coating method with low fabrication cost. Compared with the natural vertical evaporation deposition, more uniform thin film with more controlled quality can

be produced via dip coating method. The alignment direction of the coating material, coating thickness can be controlled by adjusting various coating parameters, such as drawing direction, drawing speed, concentration etc. In the study, both vertical evaporation and dip coating deposition method had been empolyed for SWCNT saturable absorber film fabrication and made comparison between them.

Figure 3.18. The DI water- SWCNT solution after 6 hours sonication.

In this experiment, we select SWCNT as raw material for saturable absorber production due to its previous demonstrated very good mode locking performance [58-60] and it can be fabricated in film structure easily. The SWCNT used for absorber fabrication was purchased from Sigma Aldrich Inc. The amide functionalized SWCNT with about 5 nm in diameter on average can be readily dissolved in DI-water. The solid SWCNT powder was added into DI water and further ultra-sonicated to form an SWCNT-DI suspension as shown in Fig. 3.18. The SWCNT concentration 0.03 wt% is close to the maximum limit as higher than that would lead to coagulation of SWCNT grains. The SWCNT-DI

suspension with 0.03 wt% was sonicated over 6 hours in a 400 W ultrasonic cleaner. Then the suspension was centrifuged at the speed of 9500 rpm for 20 minutes in order to remove SWCNTs with large bundles, only the upper portion of the centrifuged suspension is collected for the vertical evaporation and dip coating deposition methods. The quartz plate substrate for coating was first cleaned with ethanol and acetone and then sonicated to remove any impurities. Finally, substrates are treated with O_2 plasma treatment to ensure the quartz surface is ultra-hydrophilic. This process is essential as the solvent of the suspension is water in the base. Then these SWCNTs-DI suspension and substrate is ready for coating.

3.3.1 Vertical evaporation method

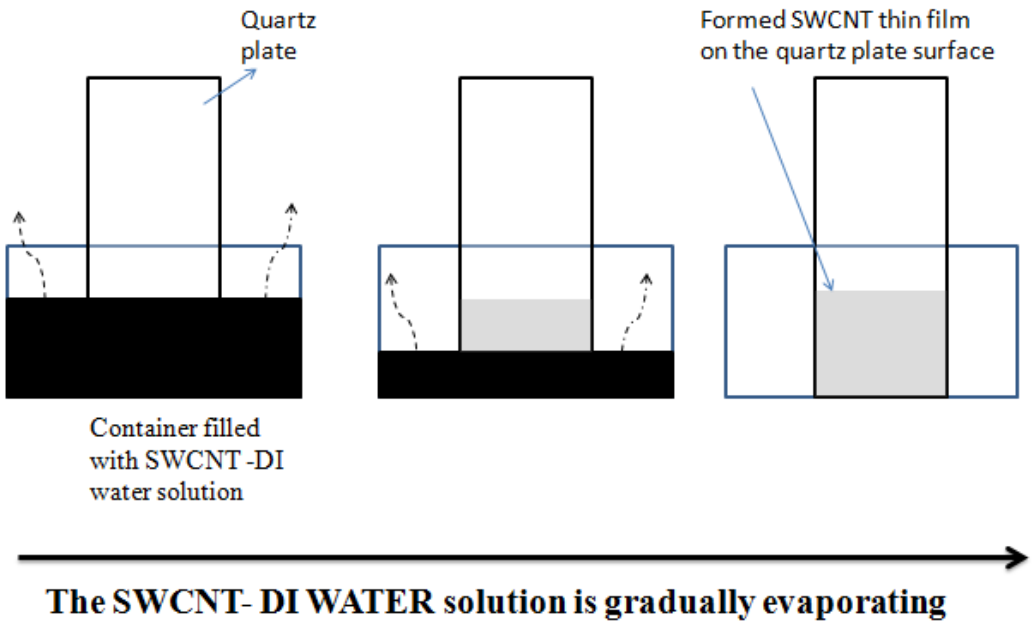

Figure 3.19. The schematic diagram of the experiment setup of vertical evaporation deposition method.

Transmission type SWCNT saturable absorber SA was fabricated for the mode locking experiments since various samples with different features can be easily changed from the laser cavity. It will also be easier to replace the damaged sample. Vice versa, for the reflective type SA, optical alignment will be much more complicated for saturable absorber sample replacement. Initially, the saturable absorber was fabricated by the vertical evaporation deposition method. The UV fused quartz plate was selected as the substrate due to its high purity and high optical transmission at 1064 nm. The quartz plate is first cleaned by acetone and ethanol ultrasonic bath for 20 minutes. Then the quartz plate was treated with

O_2 plasma to further remove the organic substance on the surface and make it ultra-hydrophilic. Then the quartz plate was placed in the container filled with 0.03 wt% SWCNT-DI water solution as shown in Fig. 3.19. The preparation method of the SWCNT-DI water solution is already discussed in the previous section. Then the setup is placed in a temperature and humidity controlled environment for over 2 weeks. After all SWCNT-DI solution evaporated, the quartz plate with the SWCNT thin film deposited on it will be collected and ready for the further test of mode locking laser pulses generation.

In the fabrication process, each SWCNT is act like a particle as shown in Fig. 3.20, that during the evaporation of the water, an evaporation flux will be generated and pull the particle (SWCNT) to the meniscus region. The SWCNT will further move to the zone which the SWCNT wet film was formed, where the SWCNT will be aligned with each other and adjusted into a regular pattern. This phenomenon is known as self-assembly [61-64]. The regularity and thickness of the formed SWCNT thin film are depending on the concentration of the SWCNT-solvent suspension and the magnitude of evaporation flux. There are few parameters affecting the magnitude of evaporation flux. They are vapor pressure, environmental temperature and relative humidity, solvent surface tension.

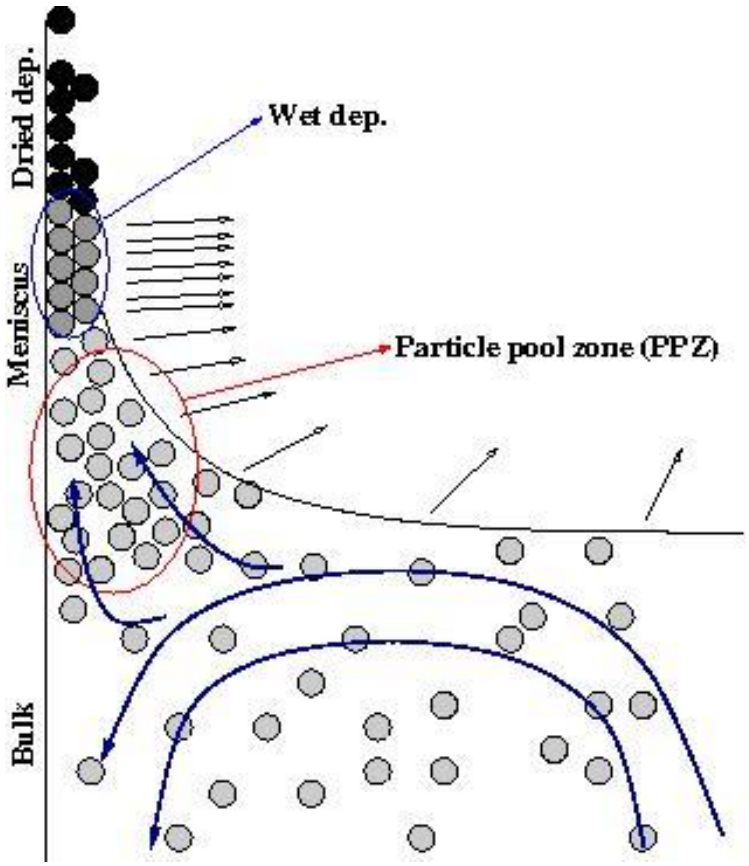

Figure 3.20. The schematic diagram of the self-assembly effects in the vertical evaporation method. [61]

The vapor pressure of DI water under the room temperature of 18℃ is 17.5 mmHg. This parameter affects the evaporation rate of the corresponding solvent. The evaporation rate will increase with vapor pressure. This will also lead to greater generated flux and more particles (SWCNT) move toward the formed film. Also, the evaporation rate will increase with the environmental temperature, but decrease with the surrounding relative humidity.

The surface tension of DI water in 18℃ room temperature is 71.97 mN/m, and the contact angle between the DI water and the O_2 plasma treated quartz plate is less than 1°. The slope of the meniscus region is determined by the surface

tension of the solvent and its attraction force to the substrate. For the smaller solvent surface tension, the slope of the meniscus region will become greater and leads to higher evaporation rate and flux of the solvent. Additionally, the withdrawn speed will also affect the slope of the meniscus region.

The weight of the suspension thin film in meniscus region as shown in Fig. 3.20 will tend to pull the materials down. If the formation speed of the suspension film in the meniscus region unable to be synchronized with the film evaporation rate, the accumulated liquid film weight will eventually pull down the suspension and SWCNT from the higher position to the lower position. Then the SWCNT will be self-assembled and dried up at the lower position and leave the high position with low density of SWCNT. This process will repeat and produce large fringe SWCNT pattern.

Samples fabricated by vertical evaporation method

Two samples were prepared by vertical evaporation method with surrounding temperature 18℃ and relative humidity 40 to 50% over the whole evaporation process. The SWCNT-DI concentration was 0.03 wt%. The fabrication time taken for samples with 17 mm in height will take around 14 days. Both produced samples look identical. One of the produced sample photo was shown in Fig. 3.21 and SWCNT pattern under optical microscope was given in Fig. 3.22.

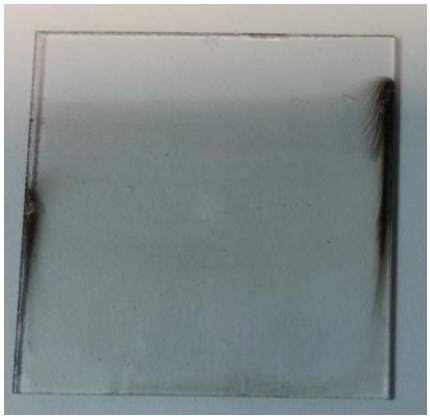

Figure 3.21. The SWCNT absorber sample produced by a vertical evaporation method (Evaporation Temperature:18℃, Relative Humidity: 40~50%, SWCNT-DI concentration:0.03wt%).

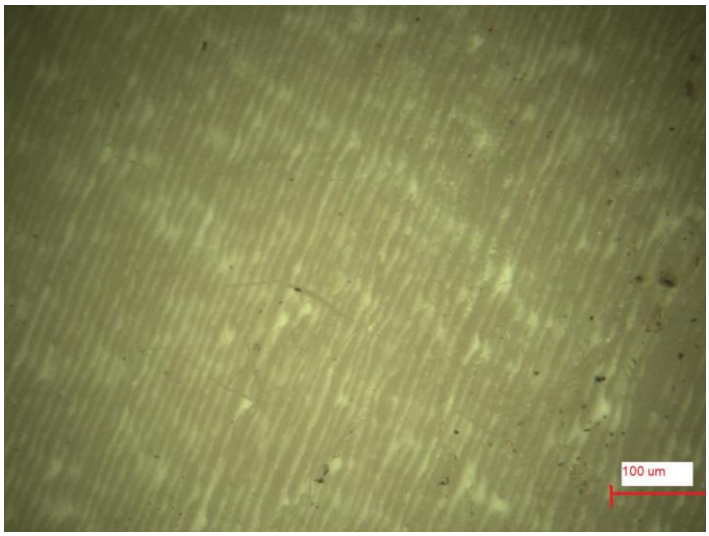

Figure 3.22 Optical microscope image of the sample produced by a vertical evaporation method (The white fringe representing the SWCNT film).

Fig. 3.22 shows fringes of the SWCNT form on top of the substrate. In this case formation of the suspension thin film in the menciscu region is generated by natural suspension evaporation. The weight of the suspension thin film in the menciscu region kept accumulated and eventually pull the suspension down to a lower position and form fringes.

Continuous SWCNT film pattern could possibly be achieved provided the conditions are optimized. However, it is very difficult and expensive to control the temperature and relative humidity over such a long period of time. Ideally, the SWCNT thin film should be in continuous form with the same thickness over the whole area so that initial transmission and stable saturable absorption performance can be achieved over the whole area. The initial transmission of the produced absorber and quartz substrate are tested and listed in Table 3.1.

Transmission of the quartz plate without SWCNT	99.0%
Transmission of the SWCNT sample	81.6%

Table 3.1. Initial Transmission of the SWCNT sample produced by a vertical evaporation method.

Then the produced sample was inserted into the position 5 mm apart from the M6 in the laser cavity given in Fig. 3.12. The absorber was fixed on a mirror holder controlled by a XYZ stage for the fine adjustment of the position and angle of the absorber to check the mode locking performance of the various position of the absorber. The absorber needs to be tiled at certain angle with respect to the optical axis to minimize the optical losses. If the SWCNT quartz plates is exactly perpendicular to the optical axis, no passive mode-locking pulses can be observed. The Brewster angle is about 15° from the vertical axis.

The optical losses can be minimized by adjusted into Brewster angle as laser beam produced from Nd:YVO_4 crystal is horizontally polarized. After some fine adjustment of the angle and position of the saturable absorber, some laser pulses train was detected with respect to the pump diode laser current of 15 A (8.4 W incident pump power) as shown in Fig. 3.23.

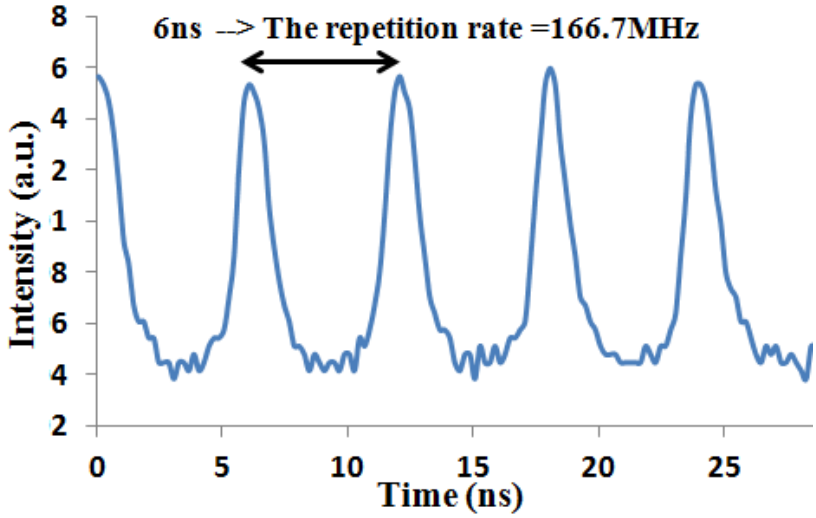

Figure 3.23. The CW mode locking pulse train obtained with respect to the pump current of 15A.

The laser operation mode with respect to various output power, pump power and current are shown in Table 3.2.

Table 3.2 The output power of the pulse train under different pumping level.

Pump current (A)	Pump power (W)	Output Power (W)	Operation mode
7.2	1.7	threshold	CW
8	2.4	0.31	CW
10	2.1	0.77	CW
12	5.8	1.34	Q-switch mode-locking
15	8.4	2.30	CW mode locking

As the pump power increases to 5.8 W, the laser output switched from CW mode to Q-switch mode-locking. Under the 5.8 W pump power, the pulse train is in Q switch mode locking mode due to the incident fluence is not high enough to fully saturate the saturable absorber. When the pump power increased to 8.4W, the pulse train produced becomes CW mode locking as the incident fluence is over the saturable fluence of the produced absorber. However, not every position of the SWCNT film can sucessfully produce passive mode-locking pulses. It may be due to the non-regular film pattern of the produced SWCNT thin film.

To brieftly conclude, although successful CW mode locking pulses was obtained by the produced absorber, but the vertical evaporation method has three main disadvantages for industrial production of the SWCNT-based absorber. Firstly, the production time is too long. As mentioned above, it generally takes two

weeks to produce a 17 mm height sample by using water as solvent. Although the process can be speed up by controlling the temperature or using highly volatile solvent but it may lead to even more irregular deposition of the SWCNT and degrade mode-locking laser stability and performance. Secondly, due to the lengthy production period, it is more difficult or more expensive to provide the optimized production conditions. Thirdly, as the solvent evaporates over time, the SWCNT concentration of the solvent will increase over time and lead to non-uniform film thickness. It is expected the SWCNT film will get thicker at the bottom part compared with the upper part. Therefore, it explains why not all the part of the produced film can successfully produce mode locking pulses. Therefore, the next stage research works focus on developing dip coating technology for the SWCNT absorber fabrication and the related research works was given in the next section.

3.3.2 Dip coating deposition

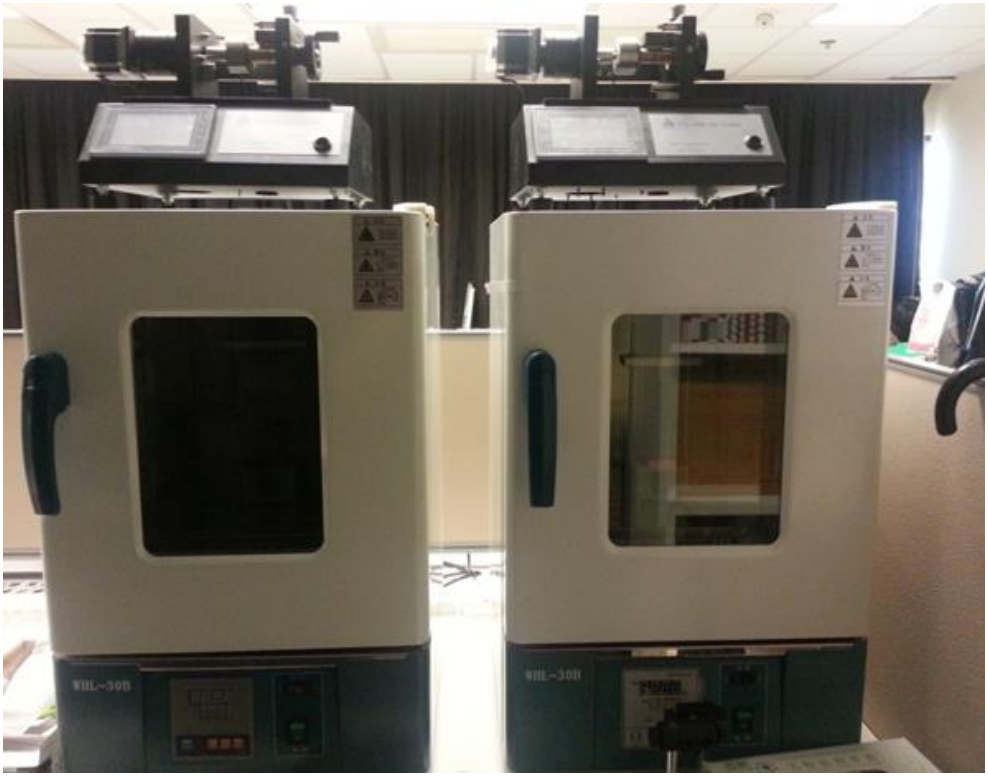

Figure 3.24. Dip coater with two different drawing speed ranges.

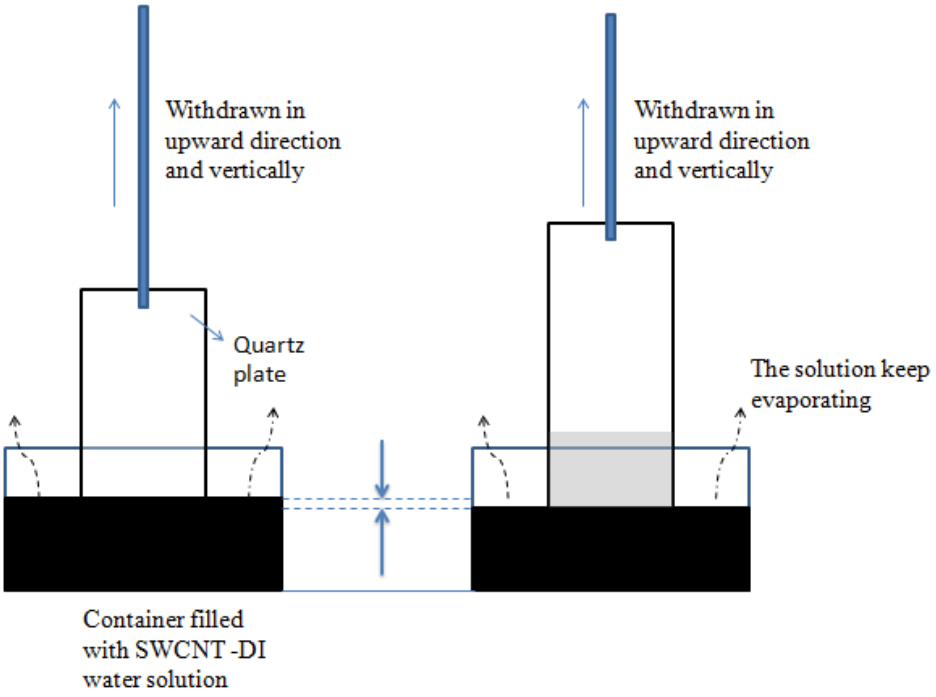

Figure 3.25 The schematic diagram of the experimental setup for dip coating SWCNT film.

The withdrawn process is controlled by a programmable dip coater as

shown in Fig 3.24. Similar to vertical evaporation deposition, a thin suspension liquid film was coated on the substrate as described in Fig. 3.20. As this liquid thin film was drawn up and evaporated, it generated a flux to drive the coating material, SWCNT to the substrate surface and allows self-assembling to form the solid pattern. The thickness of the suspension on the substrate determined the thickness and regularity of the SWCNT solid film produced. The thickness of the suspension film can be controlled by changing the substrate drawing speed, surface tension of the suspension, temperature, relative humidity, etc. For the non-colloidal solution, the suitable drawing speed tends to be higher in the range from 100 μm/s to 1 mm/s as self-assembly of the materials is not involved. However, the SWCNT-DI suspension is a colloidal solution, slower withdrawn speed is therefore needed for self-assembly of the SWCNT. The water molecules within the SWCNT-DI suspension would be pulled up and evaporated to drive and trapped the SWCNTs into the suspension thin film zone, in which the SWCNTs is self-assembled and then dry up to form a regular solid film pattern. As mentioned before, the strips pattern observed from the absorber is due to the gravitationally driven jump mechanism repeats periodically. Withdrawal of the substrate and evaporation from the container raises the height of the meniscus relative to the substrate surface. Eventually, the meniscus becomes too heavy. It

slides to a new position determined by the receding contact angle of suspension on the substrate. The time required for a meniscus to form, stretch, and jump determines the stripe spacing. Thus, it is also very important to synchronize evaporation rate with the speed of the formation of the liquid film, which is controlled by the drawing speed. Fringe separation would be too large and no continuous film was formed for drawing speed at 30 nm/s and 63 nm/s as Fig. 3.26(a) & (b) shown.

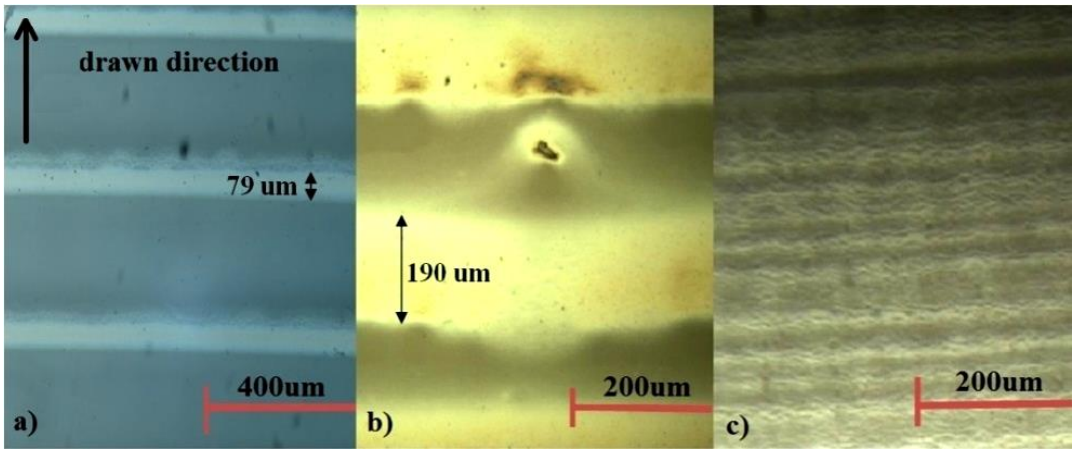

Fig.3.26. The optical microscope image of the formed SWCNT film with dipping condition of (a) 30nm/s, (b) 63nm/s and (c) 96nm/s withdrawn speed, 22 ^{o}C dipping environment temperature, 40% relative humidity and 0.03wt% SWCNT-DI suspension concentration with 0.1wt%SDS being added. (Due to the reflection of the light, the dark region has less density of SWCNT.)

As shown in Fig. 3.26 (c) and Table 3.3, the uniformity and continuity of the SWCNT film and its laser performance has been significantly improved by

increasing drawing speed up to 96 nm/s (sample c). Sample C absorber has to be used within the laser cavity to produce stable CW mode locking as shown in Table 3.3. However, with the increase of the drawing speed up to 160 nm/s, the produced SWCNT absorber has no significant changes in terms of film pattern and optical transmission, which indicates that the optimal drawing speed is close to ~100 nm/s for these drawing conditions. We expected the uniformity of the SWCNT film can be further improved by having more accurate control on the drawing temperature, humidity and more stable environment (e.g. on an anti-vibration optical table).

Sample	Withdrawn speed (nm/s)	Average fringe width (μm)	SWCNT-DI suspension conc. (wt%)	Initial Transmission at 1064nm (%)	Mode locking laser
A	30	80	0.03	78	No
B	63	195	0.03	71	UQWML
C	96	C. F.	0.03	68	SCWML
D	96	C. F.	0.015	81	SCWML

Table 3.3. The dip coating samples produced with various parameters and lasing performance. C. F. –continuous film; UQML-unstable Q-switch mode lock; SCWML-stable CW mode locking. The temperature and relative humidity were kept to be constant at 22 ^{o}C and 40 %, respectively.

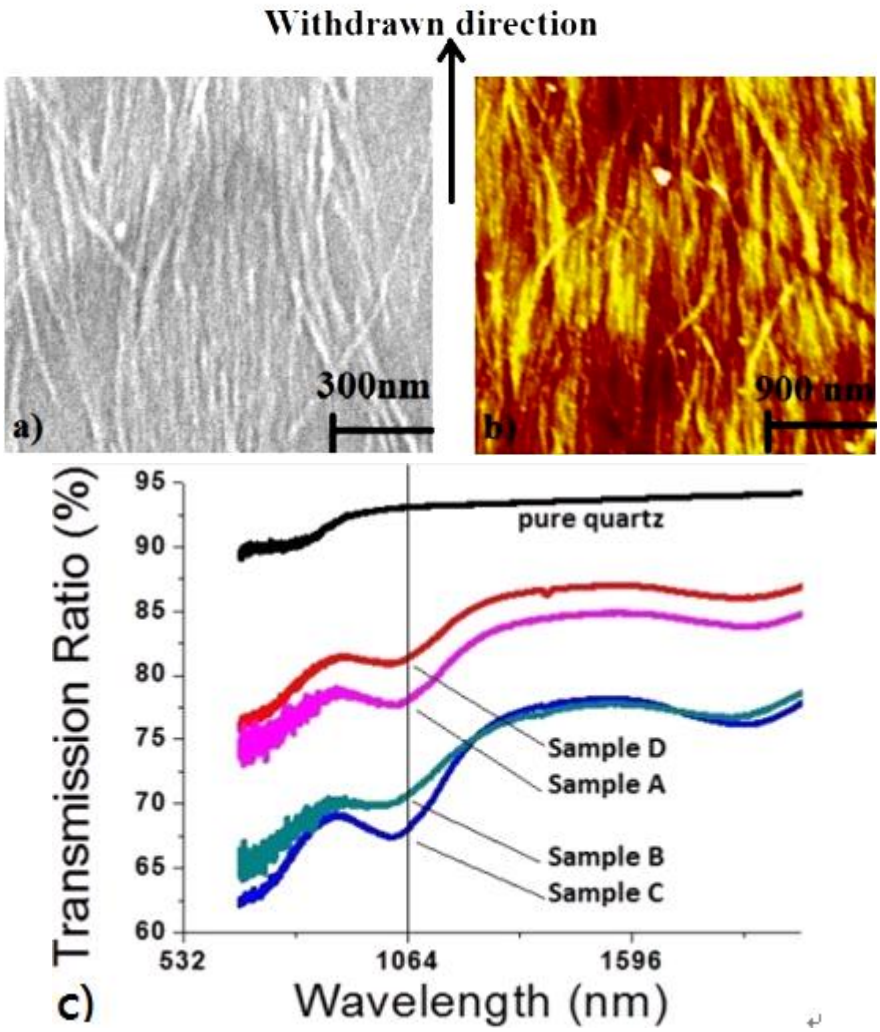

Fig. 3.27 (a)The FESEM, (b)AFM image shows the surface topography of the Sample D; (c) The Optical transmission spectra of the SWCNT-SA samples fabricated by various dipping coating conditions as shown in Table 3.3.

Sample D was produced by reducing suspension concentration to 0.015wt%, but

all other dipping parameters are remained unchanged compared with that of sample C. Then the initial transmission ratios of fabricated SWCNTs-SA samples are measured by using FTIR as shown in Fig. 3.27(c) and Table 3.3. The absorption of the sample D at 1064 nm reduces as expected when compared with sample C. Under same drawing conditions and evaporation rate of the dip coating process, the lower concentration of the SWCNT-DI suspension leads to less carbon nanotubes being trapped in the suspension thin film, thus eventually fabricating a SWCNT solid film with lower absorption. In this way, the film thickness and initial transmission of the SWCNT absorber can be changed but its film pattern and continuity remains unchanged. Fig. 3.27 (a) & (b) show the alignment of the SWCNTs on Sample D are parallel with the withdrawn direction. It proved that the SWCNT alignment direction can be controlled via the dip coating method due to the self-assembly effect, further enhancing the regularity and uniformity of the absorber, which is a unique feature when compared with absorber fabricated by other methods e.g. spin or spray coating methods. This well aligned SWCNT can serve as optical polarizer [65]. That may be potentially used to produce polarized laser output. It takes only 15 hours to produce a 2cm x 2cm continuous SWCNT thin film on a quartz substrate. In principle, the production yield can be easily enhanced by using wider substrate.

The optimal drawing speed is determined by evaporation rate, surface tension of substrate and liquid, speed of self-assembling of SWCNT. Therefore, the sample drawing speed can be further increased by adjusting temperature and humidity. The remaining suspension can be dilated and recycled for the next dip coating process, indicating its great potential for mass production.

Laser experiments and results discussion

The SWCNT saturable absorber inserted about 3 mm apart from the end 1064nm HR flat mirror to obtain high optical intensity within the mode locking laser system as illustrated in Fig. 3.12 for mode locking performance test. Fig. 3.28 shows the average output power with respect to various incident pump power and respected operational modes. The threshold for stable CW mode-locking and slope efficiency of Sample C are 7.93W and 34%. The threshold for stable CW mode-locking and slope efficiency of Sample D are 4.5W and 39%. Due to the lower insertion loss with thinner SWCNT film of Sample D, the overall mode locking performance of Sample D is better. Its maximum average output power achieved is higher up to 2.7W.

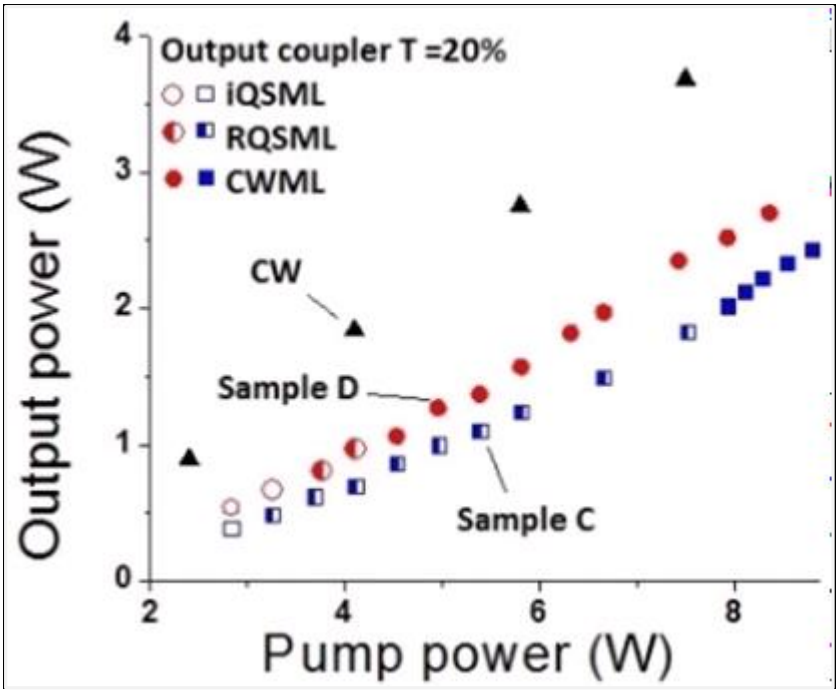

Fig.3.28. The average output power at 1064nm verse 808nm pumps power for CW and mode-locking operation. (iQSML - irregular Q-switch mode-locking mode; RQSML - regular Q-switch mode-locking mode; CWML - CW mode locking mode)

Figure 3.29(a) shows the pulse train recorded for the continuous-wave mode-locking, CWML, the operation of Sample D under 8.36 W pump power, with the repetition rate of the pulse train close to the round-trip cavity time, indicating successful CW mode locking achieved. The autocorrelation trace is shown in Fig. 3.29(b) is obtained by using an intensity autocorrelator (Femtochrome Research Inc. FR 103-XL). The measured FWHM of the pulse width is 3.1 ps for the 2.7 W maximum average output power from the mode locking system of using Sample D. The repetition rate is 167 MHz. The

estimated pulse energy and peak power are 16.1 nJ and 5.2 kW, respectively.

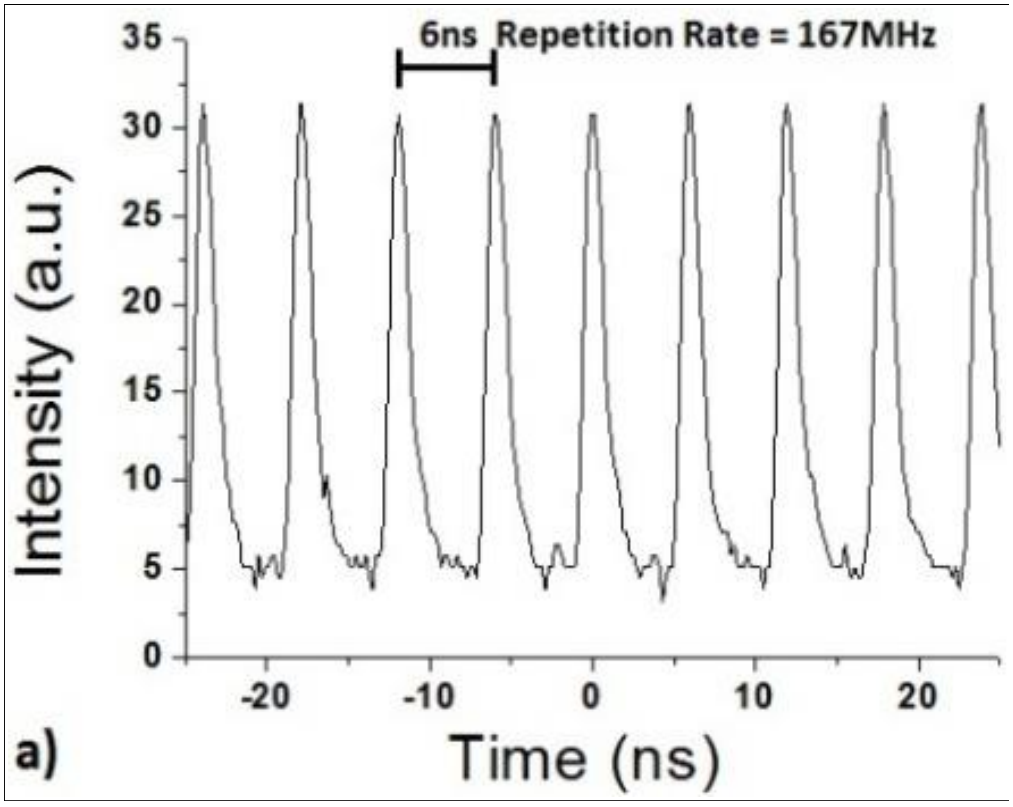

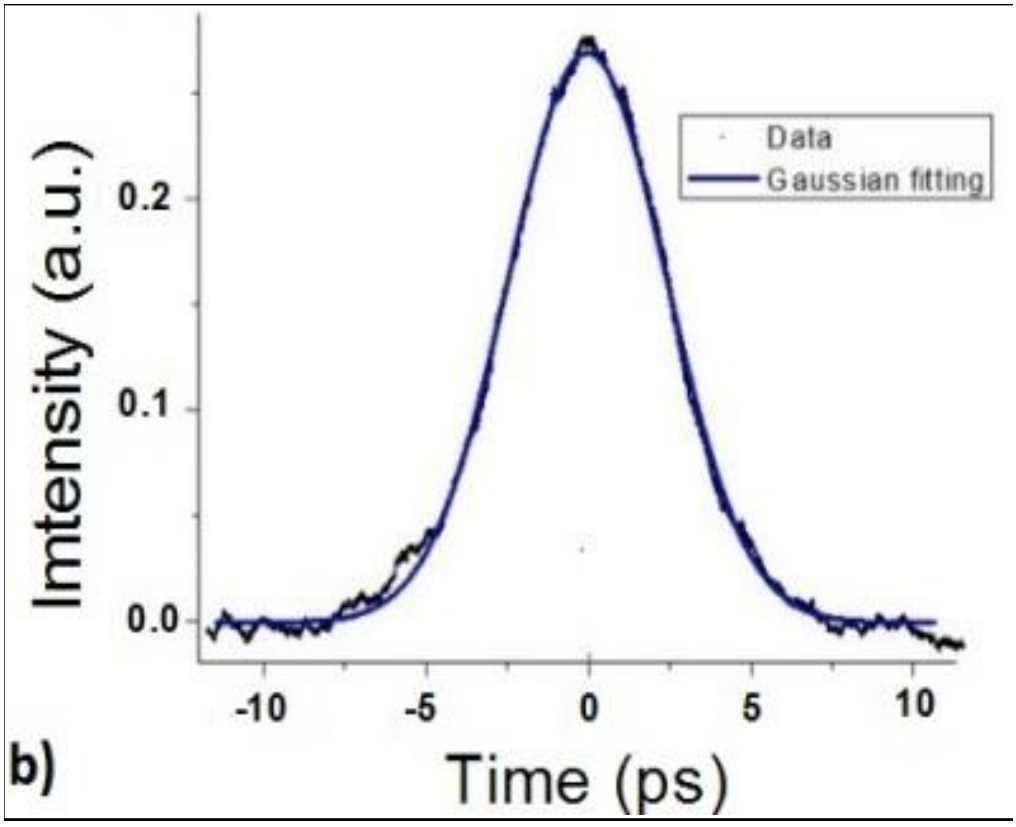

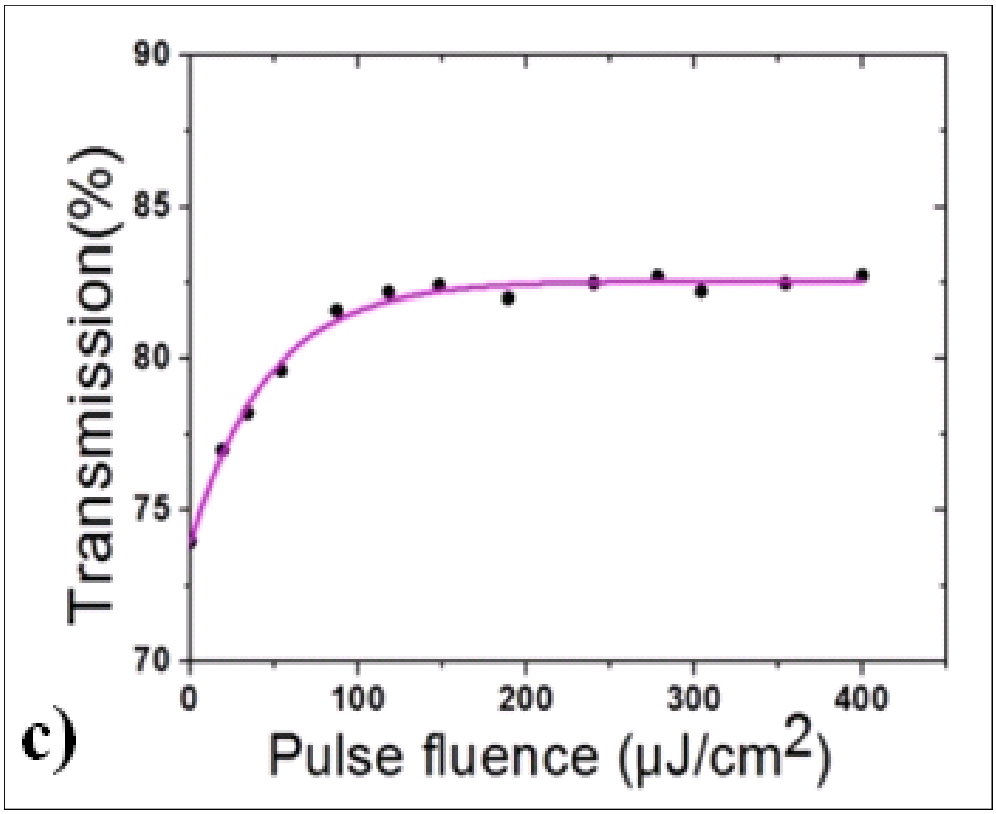

Fig. 3.29. (a) The pulse train of the CWML operation with output power of (b)The corresponding Autocorrelation spectra with respect to pump power of 8.36W. (c) The nonlinear transmission of the SWCNT-SA sample D with excitation wavelength at 1064 nm. Dots: measured data; solid curve: fitting to the data.

Previously mode-locked laser pulses with 15.7 ps pulse width was generated by using vertical evaporation deposited SWCNT absorber [58]. The pusles duration of our current system is 3.1 ps much shorter than the previous demonstration. The different pulse widths produced in these two experiments can be attributed to a various reasons, including the different average diameter of the SWCNT and alignment patterns produced by dip coating, leads to different absorption curve,

modulation depth and saturation fluence. In fact, shorter pulse width produced is expected by using saturable absorber with larger modulation depth [33]. In this experiment the measured modulation depth is 8% as shown in Fig. 3.29(c), which is higher than the modulation depth of the previous absorber used (4.4%) [58].

To brieftly conclude, SWCNT saturable absorbers were fabricated by using dip coating method under various conditions. The saturable absorbers features e.g. initial transmission ratio, film pattern was optimized by adjusting different withdrawn parameters, e.g. drawing speed, SWCNT concentration. The demonstrated fabrication method is simple, scalable, cost effective and much more suitable for industrialization. These absorbers have been successfully used within a diode pumped Nd:YVO_4 mode locking laser system operating at 1064 nm to produce high output power up to 2.7 W with continuous wave mode locking pulse duration and repetition rate of 3.1 ps and 167MHz. The transform limited pulse width is about 2 ps , which has been demonstrated in the same type of Nd:YVO_4 laser gain medium [75].The calculated pulse energy and peak power are 16.1nJ and 5.2kW, respectively.

3.4 SWCNT-PVA absorber and mode locking fiber laser pulses characterization

The fabricated SWCNT absorber has also been used to generate mode locking pulses from a fiber laser, which has the advantages of compact, cost effective, efficient, better thermal properties (usually only air cooling is needed for tens watt laser system) and more stable overall lasing performance compared with the traditional solid state laser. The intra-cavity beam radius of the fiber laser is determined by the fiber core diameter, which usually is much smaller than that of the solid state system. It provides much higher intracavity laser intensity that means higher incident fluence to the saturable absorber even with very low average output power around mW scale. Thus, stable mode-locking can be achieved easily even with lower average pumping power well above the damage threshold of the SWCNT absorber. For the above reasons, fiber laser system could be a better laser system for investigating the novel mode locking materials with laser damage threshold not been optimized yet.

In this work, fiber laser (ring cavity) with total length of about 15 meters had been built and the schematic diagram is shown in Fig. 3.30. The calculated theoretical repetition rate is around 11MHz.

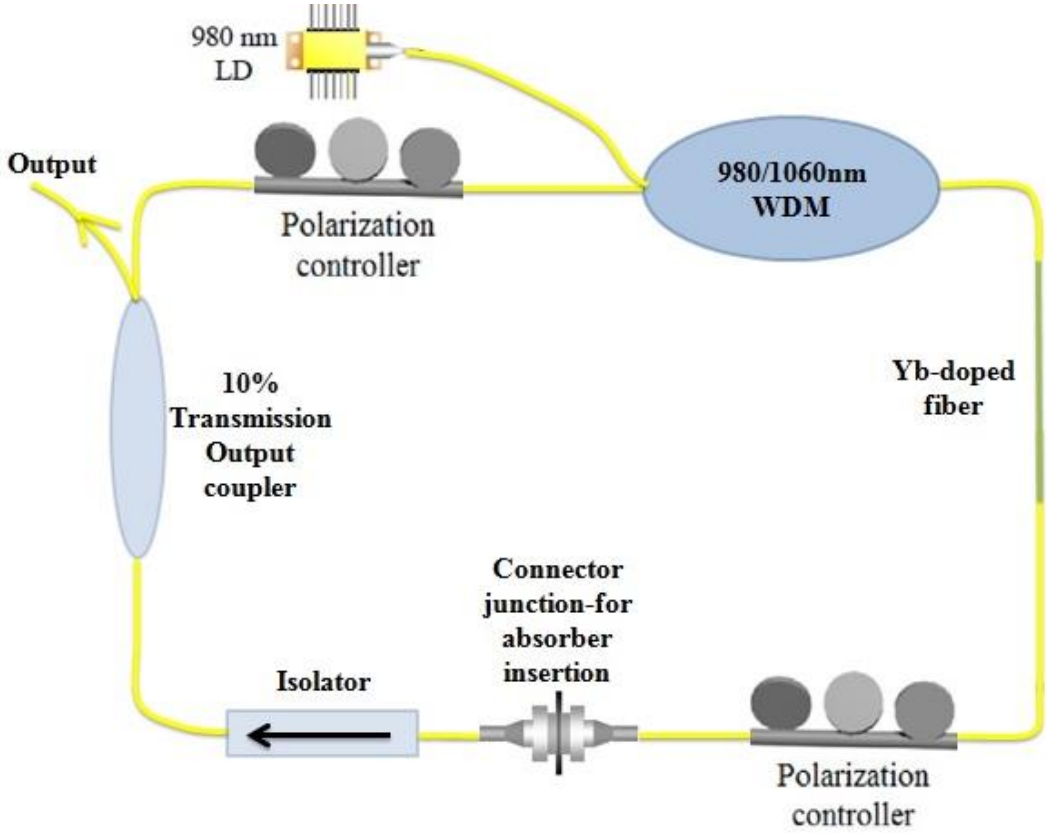

Figure 3.30. The schematic diagram of the built fiber laser system.

LIEKKI Yb doped fiber (Yb 1200-4/125) was used as the laser gain medium, which has a mode field diameter of 4.4 ± 0.8 at 1060 nm and a peak core absorption of 1200 dB/m at 976 nm. The used length of the Yb doped is 0.65m and the fiber group velocity dispersion is 24.22 ps^2/km. A 976-nm laser diode (II-IV LC96A76P-20R), with 400 mW maximum output power, was connected to a 980/1060 WDM (Thorlabs WD202E) and thus coupled the pump light into the ring cavity. An intracavity polarization-independent isolator (PI-ISO Thorlabs IO-H-1064B) was placed inside the laser cavity to ensure the unidirectional operation. An additional intra-cavity polarization controller (PCs Thorlabs FPC 024) were used to adjust the cavity polarization and birefringence in order to optimize the laser mode-locking performance.

Since it is a ring cavity setting, only transmission type saturable absorber can be

used. In this case, the 0.03 wt% SWCNT-DI solution with the fabrication procedures given in section 3.3 was also used for the absorber fabrication. However, since the absorber needed to be placed at the fiber end shown in Fig. 3.31, a SWCNT-PVA solid film was fabricated. The SWCNT-DI solution was mixed with 5 wt% PVA solution by 2:1 ratio and further stirred by a magnetic stirrer for 5 hours. Then the mixture was poured into a container and put into an oven with regulated temperature of 80℃ and relative humidity of 50%. After 12 hours evaporation inside the oven, SWCNT-PVA thin film was produced and its photo was shown in Fig. 3.32. Then this film was cut into a small piece and be attached on the end face of the FC-APC fiber connector.

Figure 3.31. And the SWCNT-PVA film coated on the connector end

Fig. 3.32: The SWCNT-PVA thin film.

The SWCNT-PVA film acts as a saturable absorber and inserted within the laser cavity. Under a pump power of 50 mW from a 976nm diode laser, CW mode-locked pulses were generated with pulse train shown in Fig. 3.33. The pulse repetition rate measured is about 10 MHz and match well with the round trip cavity time of the laser cavity.

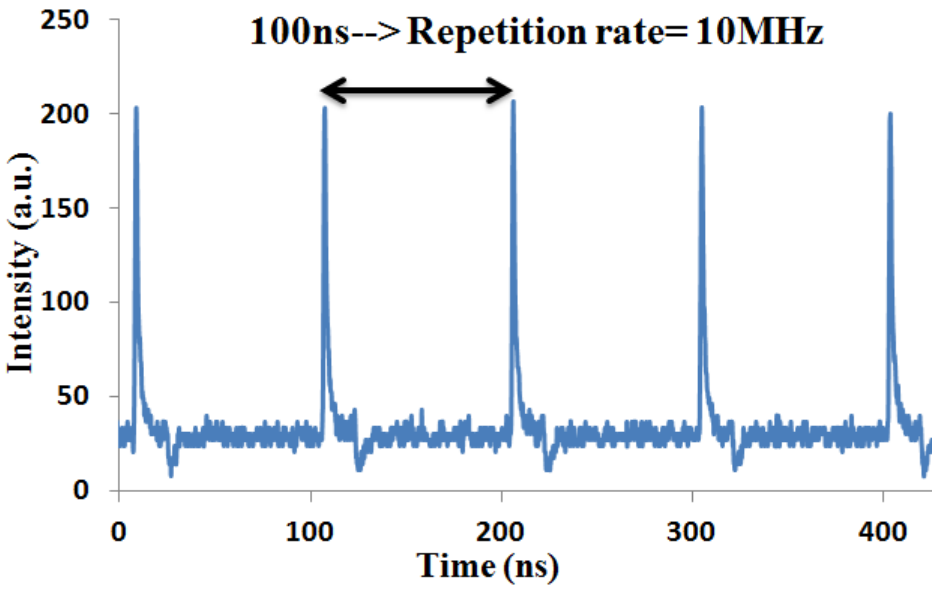

Figure 3.33. The output mode locked pulse from fibre laser system by using SWCNT-PVA absorber under 50mW pump power.

3.5 Summary

By using functional SWCNT material, different saturable absorbers have been successfully fabricated by vertical evaporation method, dip coating method and PVA oven method. The Nd:YVO_4 solid state laser and Yb doped fiber laser have been constructed and their mode locking performance were characterized by using various fabricated saturable absorbers. We have first demonstrated mode-locked end pump solid state Nd: YVO_4 laser by using SWCNT-SA which fabricated by dip coating method and published in Optics Express.

In the future research work, the relationship between the thickness, diameter and length of the SWCNT with respect to mode locking performance will be further investigated. Other novel 2D materials, such as TMDs [66-74] can be integrated with SWCNT to form a new hybrid or composite structure. For example, layer of MoS_2 or WS_2 nano particles can be coated on the SWCNT by using hydrothermal method to form a composition structure. These new structure can potentially have broad operational wavelength range or potentially enhance the mode locking performance for certain operational wavelength.

CHAPTER 4
Conclusion

4.1 Conclusion

In this thesis, I investigated different type of saturable absorber fabrication methods and the passive mode-locking effect of single-walled carbon nanotube saturable absorber which has been used within solid state Nd:YVO_4 diode pumped laser system and Yb fiber laser to successfully generate stable mode locking laser pulses by using these fabricated absorbers. Some laser intracavity laser beam profile simulation has been created for designing the laser cavity. Different from the traditional spray, spinning coating method, the first demonstrated dip coating fabrication method for the SWCNT-based absorber is an effective, low-cost method and suitable for industrial manufacturing. The method for varying the absorber initial transmission has also been demonstrated. Relatively uniform and large surface area SWCNT thin film (greater than 1cm x 1cm size) are successfully coated on quartz plate to form a transmission type saturable absorber. By adjusting the dip coating parameters, for example, the concentration of the dip coating suspension, withdrawn speed, temperature or relatively humidity of the surrounding environment, over 12% variation of the initial transmission ratio of the fabricated sample was successfully demonstrated.

The repetition rate of the laser pulse achieved is 167 MHz and the estimated pulse energy and peak power of the output pulse generated are 16.1 nJ and 5.2 kW, respectively. These research findings have been published in Optics Express. Additionally the SWCNT absorber has also been fabricated by vertical evaporation method and PVA methods and successful laser mode locking operations have also been achieved by using these fabricated absorbers.

Microfluidic device is currently a very important topic as its potential for tunable optical device and biomedical application. During my MPhil. study, a liquid lensed fiber with controllable focusing power was successfully demonstrated. By filling DI water into a hollow core of the Teflon-AF optical fiber and further applying electrical field, the core liquid will be pull out from the fiber core and formed a plano-convex lens on the fiber tip. By controlling the electric field across it, the shape, radius of curvature and focusing power of the formed liquid lens on the fiber tip can be varied. The experiment has successfully demonstrated a variation of focal length from 0.628mm to 0.111mm responding to the change of applied voltage from 0V to 3.2 kV (L = 2mm) for the Teflon AF fiber. Parabolic shape of the liquid lens was observed for voltage higher than 2.6 kV, which is a simple and practical method to produce micron sized parabolic lens as compared to traditional mechanical polishing. The research output has been

published in Optics Express as well.

4.2 Future Work

A deeper investigation of the SWCNT properties related laser mode locking performance can be done in the future. The relationship between CNT diameter, surface functional group, charity, and the mode-locking performance, e.g. laser threshold, effieint can be studied systemically. These study could potentailly leads to better design of th carbon nanotube based saturable absorber for further mininize the non-saturable loss of the fabricated absorber and also shorten the pulse duration. The SWCNT-SA fabricated can operate stably for about 15 to 20 minutes, long enough for recording all data needed for the experiment. In the next stage, we aim to develop a practical ensheilding method to isolate the SWCNT thin film from atmosphere in order to further increase the damage threshold of the fabricated SWCNT-SA.

Recently two-dimensional Transition-Metal Dichalcogenide (TMDs) as saturable absorber have attracted great research interests due to its broad range of bandgap structures and other attractive nonlinear optoelectronic property when they are in mono or few-layer nanosheets form. Layered TMDs has the stoichiometry of MX_2, which each layer compose of a single plane hexagonally arranged

transition metal (M) atom carried between two hexagonal planes of chalcogen atom. Their bandgap and properties can be modified by changing the different combination of M and X elements. We are preparing the fabrication of new type of saturable absorber by using TMDs based materials which can potentially be used for either solid state or fiber laser mode locking or Q-switching.

The lensed liquid core fiber with electrical controllable focus can be integrated within the fiber laser system to produce active Q-switching. It will be an interesting research project to demonstrate the active Q-switching by using this lensed liquid fiber as Q-swicther.

Appendix

ABCD matrix program code(for simulation the radius variation of the lasing mode with the solid state laser cavity):

```
% lasing cavity with thermal lensing effects introduced by the pumped
% crystals in (mm)
clc;
clear;
R1=;     %M1
R2=;     %M2 concave mirror
R3=;     %M3 1064HR
R4=;    %M4 concave mirror
R5=;     %M5 808HT 1064HR
R6=;     %thermal lensing
R7= ;     %Ouput coupler Transmittion mirror T=20% with 2 degree cutting
n=1;
lambda=1.064*10^-3;        % wavelength in mm scale

d1=;     %Distance between M1 and M2
d2=;     %Distance between M2 and M3
d3=;     %Distance between M3 and M4
d4=;     %Distance between M4 and M5
d5=;          %Distance between M5 and m6
d6=;         %Distance between M6 and output coupler


m=d1+d2+d3+d4+d5+d6;    %Total cavity length (mm)

for x=0:1:m

    if (x>=0&&x<=d1) %begin from any one point of the back of M1 SESAM
      m1=[1,x;0,1];
      m2=[1,0;-2/R1,1];
      m3=[1,d1;0,1];
      m4=[1,0;-2/R2,1];
      m5=[1,d2;0,1];
      m6=[1,0;-2/R3,1];
      m7=[1,d3;0,1];
```

```
m8=[1,0;-2/R4,1];
m9=[1,d4;0 1];
m10=[1,0;-2/R5,1];
m11=[1,d5;0,1];
m12=[1,0;-2/R6,1];
m13=[1,d6;0,1];%
m14=[1,0;-2/R7,1];%
m15=[1,d6;0,1];%
m16=[1,0;-2/R6,1];%
m17=[1,d5;0,1];
m18=[1,0;-2/R5,1];
m19=[1,d4;0 1];
m20=[1,0;-2/R4,1];
m21=[1,d3;0,1];
m22=[1,0;-2/R3,1];
m23=[1,d2;0,1];
m24=[1,0;-2/R2,1];
m25=[1,d1-x;0,1];


elseif (x>d1&&x<=d1+d2)    %begin from any one point of the back of M2
m1=[1,x-d1;0,1];
m2=[1,0;-2/R2,1];
m3=[1,d1;0,1];
m4=[1,0;-2/R1,1];
m5=[1,d1;0,1];
m6=[1,0;-2/R2,1];
m7=[1,d2;0,1];
m8=[1,0;-2/R3,1];
m9=[1,d3;0 1];
m10=[1,0;-2/R4,1];
m11=[1,d4;0,1];
m12=[1,0;-2/R5,1];
m13=[1,d5;0,1];
m14=[1,0;-2/R6,1];
m15=[1,d6;0,1];%
m16=[1,0;-2/R7,1];%
m17=[1,d6;0,1];%
```

```
    m18=[1,0;-2/R6,1];%
    m19=[1,d5;0 1];
    m20=[1,0;-2/R5,1];
    m21=[1,d4;0,1];
    m22=[1,0;-2/R4,1];
    m23=[1,d3;0,1];
    m24=[1,0;-2/R3,1];
    m25=[1,d1+d2-x;0,1];

  elseif (x>d1+d2&&x<=d1+d2+d3)
    m1=[1,x-d1-d2;0,1];          %begin from any one point of the back of M3
    m2=[1,0;-2/R3,1];
    m3=[1,d2;0,1];
    m4=[1,0;-2/R2,1];
    m5=[1,d1;0,1];
    m6=[1,0;-2/R1,1];
    m7=[1,d1;0,1];
    m8=[1,0;-2/R2,1];
    m9=[1,d2;0 1];
    m10=[1,0;-2/R3,1];
    m11=[1,d3;0,1];
    m12=[1,0;-2/R4,1];
    m13=[1,d4;0,1];
    m14=[1,0;-2/R5,1];
    m15=[1,d5;0 1];
    m16=[1,0;-2/R6,1];
    m17=[1,d6;0,1];%
    m18=[1,0;-2/R7,1];%
    m19=[1,d6;0,1];%
    m20=[1,0;-2/R6,1];%
    m21=[1,d5;0,1];
    m22=[1,0;-2/R5,1];
    m23=[1,d4;0,1];
    m24=[1,0;-2/R4,1];
    m25=[1,d1+d2+d3-x;0,1];

elseif (x>d1+d2+d3&&x<=d1+d2+d3+d4)
    m1=[1,x-d1-d2-d3;0,1];    %begin from any one point of the back of M4
```

```
m2=[1,0;-2/R4,1];
m3=[1,d3;0,1];
m4=[1,0;-2/R3,1];
m5=[1,d2;0,1];
m6=[1,0;-2/R2,1];
m7=[1,d1;0,1];
m8=[1,0;-2/R1,1];
m9=[1,d1;0 1];
m10=[1,0;-2/R2,1];
m11=[1,d2;0,1];
m12=[1,0;-2/R3,1];
m13=[1,d3;0,1];
m14=[1,0;-2/R4,1];
m15=[1,d4;0 1];
m16=[1,0;-2/R5,1];
m17=[1,d5;0,1];
m18=[1,0;-2/R6,1];
m19=[1,d6;0,1];%
m20=[1,0;-2/R7,1];%
m21=[1,d6;0,1];%
m22=[1,0;-2/R6,1];%
m23=[1,d5;0,1];
m24=[1,0;-2/R5,1];
m25=[1,d1+d2+d3+d4-x;0,1];

elseif (x>d1+d2+d3+d4&&x<=d1+d2+d3+d4+d5)
m1=[1,x-d1-d2-d3-d4;0,1];    %begin from any one point of the back of M5
m2=[1,0;-2/R5,1];
m3=[1,d4;0,1];
m4=[1,0;-2/R4,1];
m5=[1,d3;0,1];
m6=[1,0;-2/R3,1];
m7=[1,d2;0,1];
m8=[1,0;-2/R2,1];
m9=[1,d1;0 1];
m10=[1,0;-2/R1,1];
m11=[1,d1;0,1];
m12=[1,0;-2/R2,1];
```

```
m13=[1,d2;0,1];
m14=[1,0;-2/R3,1];
m15=[1,d3;0 1];
m16=[1,0;-2/R4,1];
m17=[1,d4;0,1];
m18=[1,0;-2/R5,1];
m19=[1,d5;0,1];
m20=[1,0;-2/R6,1];
m21=[1,d6;0,1];%
m22=[1,0;-2/R7,1];%
m23=[1,d6;0,1];%
m24=[1,0;-2/R6,1];%
m25=[1,d1+d2+d3+d4+d5-x;0,1];


else
m1=[1,x-d1-d2-d3-d4-d5;0,1]; %begin from any one point of the back of
M5
m2=[1,0;-2/R6,1];
m3=[1,d5;0,1];
m4=[1,0;-2/R5,1];
m5=[1,d4;0,1];
m6=[1,0;-2/R4,1];
m7=[1,d3;0,1];
m8=[1,0;-2/R3,1];
m9=[1,d2;0 1];
m10=[1,0;-2/R2,1];
m11=[1,d1;0,1];
m12=[1,0;-2/R1,1];
m13=[1,d1;0,1];
m14=[1,0;-2/R2,1];
m15=[1,d2;0 1];
m16=[1,0;-2/R3,1];
m17=[1,d3;0,1];
m18=[1,0;-2/R4,1];
m19=[1,d4;0,1];
m20=[1,0;-2/R5,1];
m21=[1,d5;0,1];%
```

```
        m22=[1,0;-2/R6,1];%
        m23=[1,d6;0,1];%
        m24=[1,0;-2/R7,1];%
        m25=[1,d1+d2+d3+d4+d5+d6-x;0,1];
        end

M=m1*m2*m3*m4*m5*m6*m7*m8*m9*m10*m11*m12*m13*m14*m15*m1
6*m17*m18*m19*m20*m21*m22*m23*m24*m25;
        a=M(1,1);
        b=M(1,2);
        c=M(2,1);
        d=M(2,2);
        if (abs((a+d)/2)<=1)
            w(n)=sqrt(lambda*abs(b)/(pi*sqrt(1-((a+d)/2)^2)));
            y(n)=x;
            z(n) =abs((a+d)/2);
            n=n+1;
        end
end
plot(y,w,'r');
hold on;
xlabel('Position within the laser cavity (mm)');
ylabel('Lasing mode radius (mm)');
title('Lasing mode radius for the 4 mirror cavity')
plot(y,z,'r');
hold on;
Y = y';
W = w';
C = horzcat(Y, W);
xlswrite('LD1.xls', C);
```

Derivation for equation 2.2 - 2.5

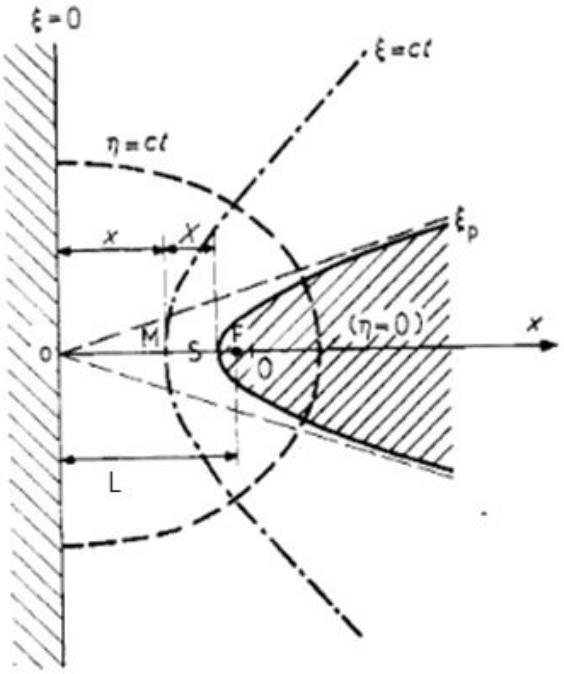

Figure 5.1 Representation of a point-plane configuration with involve of different parameter.[15].

By using hyperboloid approximation, the tip is generated by the hyperbola of equations rotating around the x axis,

$$x = L \sin \zeta \cosh \eta$$

$$y = L \cos \zeta \sinh \eta \qquad (5.1)$$

Equations (5.1) shows two orthogonal confocal sets of ellipses and hyperbolas. Since only the hyperbolas is considered, ζ is regarded as the parameter defining the hyperbola. Particular values of ζ are,

$$\zeta = 0 \quad (x = 0) \qquad As\ Oy\ axis\ generating\ the\ plane$$

ζ

$= \frac{\pi}{2}$ $(y = 0)$ $As\ Ox\ axis\ generatingan\ infinitely\ sharp\ hyperbola$

η, which is the parameter defining a particular point on the hyperbola defined by ζ. If two of the hyperbolas are equipotential surfaces all of the hyperbolas of the set are also equipotentials. Besides if the origin of the potential is taken at the plane x = 0 (ζ = O) the potential V(ζ) of the hyperbola of parameter ζ is

$$V(\ \zeta\ ) = C\ \text{In tan}\ (\frac{\zeta}{2} + \pi/4) \qquad (5.2)$$

C is a constant depending on the applied voltage. The flux lines of the field generate a family of ellipsoids of revolution orthogonal to the hyperboloids, and the value of the electric field at point (ζ, η) is

$$E(\ \zeta,\ \eta\ ) = \frac{C}{L\ \cos\ \zeta(cosh^2\eta - sin^2\zeta)^{1/2}} \qquad (5.3)$$

C is obtained by the assumption that the point is sharp, the corresponding value of ζ is close to π / 2 . If *V* is the potential of the point, we obtain *V* (π /2 - ϵ) = V, with $\epsilon \ll 1$, by using equation (5.2)

$$V = C\ \text{In tan}\ (\frac{\pi}{2} - \frac{\epsilon}{2}) = C\ \text{In cot}\frac{\epsilon}{2}$$

$$V = C\ \text{In}(\frac{2}{\epsilon} - \frac{\epsilon}{6} + \cdots) \simeq C\ \text{In}\frac{2}{\varepsilon} \qquad (5.4)$$

and

$$V(\zeta) \simeq V \quad \frac{\text{In } \tan(\frac{\zeta}{2}+\frac{\pi}{4})}{\text{In}(\frac{2}{\epsilon})} \qquad (5.5)$$

The field at any point M of the tip axis (η =0) between the tip and the plane can be calculated by let η =0 in equation 5.3, which it obtain,

$$\text{E}(\zeta\ ,0) = \frac{C}{Lcos^2\zeta} \qquad (5.6)$$

as x = a sin ζ if η =0, then

$$\text{E}(x) = \frac{aC}{L^2-x^2} \qquad (5.7)$$

Consider of Figure 5.1, the abscissa of the tip apex S is

$$\text{x}_\text{s} = \text{L sin } \zeta_\text{s} = \text{L cos } \epsilon \simeq \text{L}(1-\frac{\epsilon^2}{2}) \qquad (5.8)$$

with distance X between point M and the tip apex is

$$\text{X} = \text{x}_\text{s} - x \simeq \text{L}\left(1-\frac{\epsilon^2}{2}\right) - x \qquad (5.9)$$

&

$$\text{E(X)} = \frac{\text{LC}}{\left(\text{X}+\frac{\text{L}\epsilon^2}{2}\right)(2\text{L}-\text{X}-\frac{\text{L}\epsilon^2}{2})} \qquad (5.10)$$

with expanding the denominator to the second power in E, E(X) reduces to

$$\text{E(X)} \simeq \frac{\text{LC}}{\text{X}(2\text{L}-\text{X})+(\text{L}-\text{X})\text{L}\epsilon^2} \qquad (5.11)$$

by expanding the equations of the hyperbola and that of a circle of radius r around the common apex x = x_s = L cos ϵ and identifying both expansions, that the radius of curvature of the hyperbola is

$$\text{r} = \text{L}\epsilon^2$$

As algebraic manipulation:

$$C = \frac{V}{\ln\ \{2(\frac{L}{r})^{\frac{1}{2}}\}}$$

it shows,

$$E(X) = \frac{L \cdot V}{X(2L - X) + (L - X)r} \cdot \frac{1}{In[2(L/r)^{1/2}]} \qquad (2.2)$$

Laser mode of the Nd:YVO4 laser:

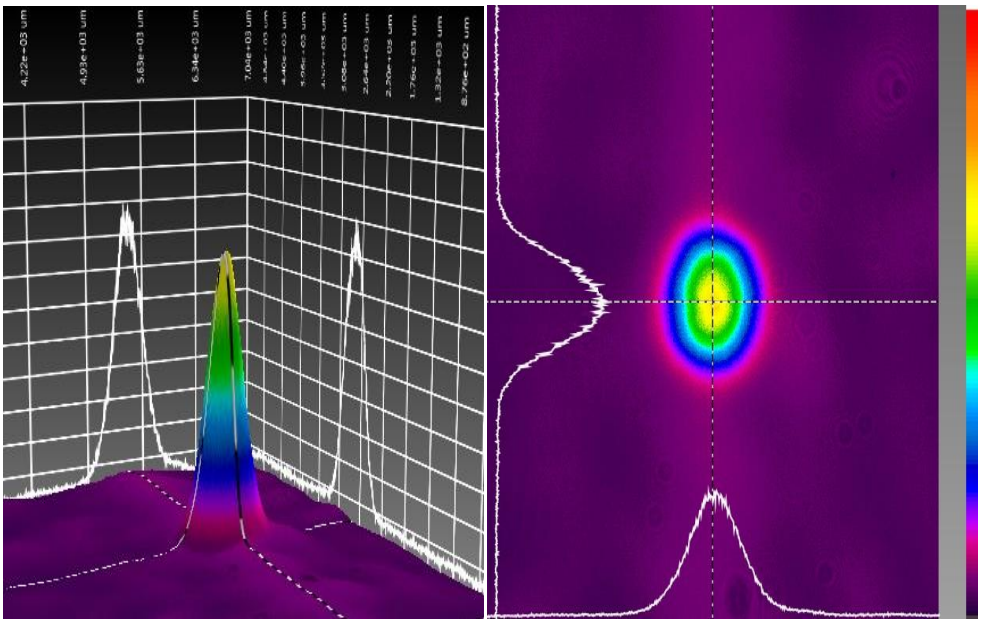

Figure 5.2 Beam profile of the Nd:YVO_4 laser

References

1. C. L. Bliss, J. N. McMullin, and C. J. Backhouse, “Rapid fabrication of a microfluidic device with integrated optical waveguides for DNA fragment analysis” Lab Chip, vol. 7, pp. 1280–1287, 2007.
2. Han Zhang, Stephane Virally, Qiaoliang Bao, Loh Kian Ping, Serge Massar, Nicolas Godbout, Pascal Kockaert, “Z-scan measurement of the nonlinear refractive index of graphene”, Optics Express, **37**(11), 1856-1858 (2012)
3. K. V. Kandidov, O. G. Kosareva, I. S. Golubtsov, W. Liu, A. Becker, N.Akozbek, C. M. Bowden, S.L. Chin, “Self-transformation of a powerful femtosecond laser pulse into a white-light laser pulse in bulk optical media(or Supercontinuum generation”, Appl. Phys. **77**, 149-165 (2003)
4. Bozolan, C.J.S. De Matos, C.M.B. Cordeiro, E.M.dos Santos and J. Travers, “Supercontinuum generation in a water-core photonic crystal fiber”, Opt. Express **16** (13), 9671-9676(2008).
5. C. Martelli, J. Canning, K. Lyytikainen, N. Groothoff, ‘Water-core Fresnel fiber’, Opt. Express , vol. 13, no. 10, pp. 3890-3895, 2005.
6. P. Dress, M. Belz, K. F. Klein, T.V. Grattan, H. Franke, “Water-core waveguide for pollution measurements in the deep ultraviolet”, Appl. Optics , vol. 37, no. 21, pp. 4991-4997, 1998.
7. U. C. Paek and A. L. Weaver, “Formation of a Spherical Lens at Optical Fiber Ends with a CO2 Laser” Appl. Opt., vol. 14, pp. 294-298, 1975.
8. Kato, Daisuke, “Light coupling from a stripe-geometry GaAs diode laser into an optical fiber with spherical end” J. Appl. Phys., vol. 44, pp. 2756, 1973.
9. Murakami, Yasuji, “Microlens tipped on a single-mode fiber end for InGaAsP laser coupling improvement” Electronics Letters., vol. 16, pp. 321 – 322, 1980.
10. Y. T. Tseng, J. B. Huang and W. J. Su, “Fabricating lensed fiber using a novel polishing method” J. Manuf. Sci. Eng. , vol. 131, pp. 041016, 2009.
11. S. I. E. Lin, “A lensed fiber workstation based on the elastic polishing plate method,” Precis. Eng. vol. 29, pp. 146–150, 2005
12. A. G. V. Engen, S. A. Diddams, and T. Clement, “Dispersion measurements of water with white-light interferometry,” Appl. Opt., vol. 37, pp. 5679-5686 , 1998.
13. Chun-Yin Tang, Gongxun Bai, Kwok Lung Jim, Xuming Zhang, Kin Hung Fung, Yang Chai, Yuen H. Tsang, Jianquan Yao, and Degang Xu," Lensed Water-Core

Teflon-Amorphous Fluoroplastics Optical Fiber," J of Lightwave Techno. 32(8), 1538-1542 (2014).

14. G.F. Zheng, W.W. Li, X. Wang, H. Wang, D.H. Sun and L.W. Lin, “Experiment and simulation of coiled nanofiber deposition behavior from near-field electrospinning”, NEMs, 284-288(2010).
15. R. Coelhot and J. Debeaus, “Properties of the tip-plane configuration”, J. Phys. D: Appl.Phys.4(9), 1266-1280(1971)
16. Kuo Yung Hung et al, “Electrostatic Force Modulated Microaspherical Lens for Optical Pickup Head”, J. Micromech Sys. 17, 370-380 (2008).
17. X. Cao, M. Jahazi, J.P. Immarigeon, W. Wallace, "A review of laser welding techniques for magnesium alloys", J. of Mat. Proc. Techno., 171(**2**), 188–204(2006).
18. K.Y. Benyounis, A.G. Olabi, M.S.J. Hashmi, "Effect of laser welding parameters on the heat input and weld-bead profile", J. of Mat.Pro. Techno., 164–165, 978–985 (2005).
19. A. Ivarsona, J. Powella, b, J. Kamaluc, C. Magnusson, "The oxidation dynamics of laser cutting of mild steel and the generation of striations on the cut edge", J. of Mat. Proc.Techno., 40(**3–4**), 359–374 (1994).
20. J.Senthil Selvan, K. Subramanian, ,A.K. Nath, "Effect of laser surface hardening on En18 (AISI 5135) steel", J. of Mat. Proc.Techno., 91(**1–3**), 29–36(1999).
21. N. Bärsch, K. Körber, A. Ostendorf, K.H. Tönshoff, "Ablation and cutting of planar silicon devices using femtosecond laser pulses," Appl, Phys. A, 77(**2**), 237-242(2003).
22. L. Qi, K. Nishii, M. Yasui, H. Aoki, and Y. Namba, “Femtosecond laser ablation of sapphire on different crystallographic facet planes by single and multiple laser pulses irradiation,” Opt. Laser Eng. 48(**10**),1000-1007(2010).
23. Ihtesham H. Chowdhury and Xianfan Xu, " Heat transfer in Femtosecond laser processing of metal," Numerical Heat Transfer, Part A 44,219–232(2003).
24. Ursula Keller, "Recent developments in compact ultrafast lasers," Nature 424, 831-838 (2003).
25. Steven Hypsh and Geoff Shannon, " Faster Laser Processing for Medical Devices," welding design & Fabrication, (2014).
26. Lonnie Lucas and Jim Zhang, " Femtosecond laser micromachining: A back-to-basics primer," Industrial Laser Solutions(2012).
27. C.Y. Chien, M.C. Gupta," Pulse width effect in ultrafast laser processing of materials", Appl. Phys. A 81, 1257–1263 (2005).
28. Rafael R. Gattass and Eric Mazur, " Femtosecond laser micromachining in transparent materials" Nature photonics 2 , 219-225(2008).
29. Shen, N. et al., "Ablation of cytoskeletal filaments and mitochondria in live cells using a femtosecond laser nano scissor," Mech. Chem. Biosystems 2, 17–25 (2005).

30. S. L. Marcus: "Photodynamic therapy of human cancer: clinical status, potentialand needs", in Future Directions and Applications in Photodynamic Therapy,C. J. Gomer (ed.), Proc. SPIE 18-6, Soc. Photo-Opt. Instrum. Eng., 5-56(1990).
31. S. Svanberg," Some Medical and Biological Applications of Ultrafast Lasers" Ultrafast Optics 95, pp 437-448(2004).
32. W. E. Lamb Jr., “Theory of an optical laser”, Phys. Rev. 134 (6A), A1429 (1964)
33. Hermann A. Haus ,"Theory of mode locking with a fast saturable absorber," J. Appl. Phys. 46, 3049-3058 (1975).
34. Sze Y. Set et al, " Laser Mode Locking Using a Saturable Absorber Incorporating Carbon Nanotubes," J. of Lightwave Techno., 22(1), 51-56(2004).
35. T. R. Schibli, K. Minoshima et al, " Ultrashort pulse generation by saturable absorber mirrors based on polymer-embedded carbon nanotubes," Opt. Exp. 13(20), 8025-8031(2005).
36. W. R. Rapoport and C. P. Khattak," Titanium sapphire laser characteristics," Appl. Opt. 27(13), 2677-2684(1988)
37. Rosa Ana Perez-Herrera and Manuel Lopez-Amo, "Current Developments in Optical Fiber Technology," chapter 17, (2013). (ISBN 978-953-51-1148-1)
38. Sutter, D. H.et al.,” Semiconductor saturable-absorber mirror-assisted Kerr-lens mode-lockedTi:sapphire laser producing pulses in the two-cycle regime,” Opt. Lett.24(63),631–633 (1999).
39. Ell, R.et al.Generation of 5-fs pulses and octave-spanning spectra directly from a Ti:sapphire laser.” Opt. Lett.26,373–375 (2001).
40. Dr. Rüdiger Paschotta, Mode Locking, Retrieved from https://www.rp-photonics.com/mode_locking.html
41. H. Klann, J. KuhlD. Von Der Linde, “Highly stable acoustic-optic mode-locking using active feedback,” Opt. Comm. 38, (5–6), 390-392 (1981).
42. H J Baker and T A King, ” Electro-optic mode-locking of the iodine photodissociation laser.” J. of Phys. E: Scient. Instru. 9(4),(1975).
43. Dr. Rüdiger Paschotta, Active mode locking, Retrieved from https://www.rp-photonics.com/active_mode_locking.html.
44. Ken Kashiwagi and Shinji Yamashita," Optical Deposition of Carbon Nanotubes for Fiber-based Device Fabrication"'DOI: 10.5772/39546
45. Shank, C. V. "Ultrashort Laser Pulses and Applications" (ed. Kaiser, W.) Chapter 2 (Springer,Heidelberg, 1988).
46. Diels, J.-C. "Dye lasers principles: with applications" (eds Duarte, F. J. and Hillman, L. W.) 41–132(Academic Press, Boston, 1990).
47. Shank, C. V. & Ippen, E. P. "Subpicosecond kilowatt pulses from a modelocked cw dye laser," Appl. Phys.Lett. 24, 373–375 (1974)

48. Fork, R. L., Cruz, C. H. B., Becker, P. C. & Shank, C. V." Compression of optical pulses to sixfemtoseconds by using cubic phase compensation," Opt. Lett. 12, 483–485 (1987).
49. Moulton, P. F. "Spectroscopic and laser characteristics of Ti:Al2O3,". J. Opt. Soc. Am. B 3, 125–132(1986).
50. Spence, D. E., Kean, P. N. & Sibbett, W. in Conference on lasers and electro-optics (CLEO) CPDP10(OSA/IEEE LEOS, Anaheim, California, 1990).
51. Jonghan Jin and Seung-Woo Kim, "Advances in Solid State Lasers Development and Applications," book edited by Mikhail Grishin, ISBN 978-953-7619-80-0, Published: (2010).
52. Arnero, " Kerr-lens modelocking," Retrieved from https://en.wikipedia.org/wiki/Kerr-lens_modelocking9 (2007)
53. U. Keller, D. A. B. Miller, G. D. Boyd, T. H. Chiu, J. F.Ferguson, and M. T. Asom, "Solid state low-loss intracavitysaturable absorber for Nd-YLF lasers and antiresonant semiconductor Fabry-Perot saturable absorber," Opt. Lett.17, 505-507 (1992).
54. Vazquez-Zuniga Luis A., Jeong Yoonchan," Wavelength-Tunable, Passively Mode-Locked Erbium-Doped Fiber Master-Oscillator Incorporating a Semiconductor Saturable Absorber Mirror," J. of the Opti. Soc. of Korea 17(2), 117~129(2013).
55. R. Fluck, R. Haring, R. Paschotta, E. Gini, H. Melchior, and U. Keller, "Eyesafe pulsed microchip laser using semiconductor saturable absorber mirrors," Appl. Phys. Lett. 72(25), 3273-3275(1998).
56. W. Koechner," Thermal Lensing in a Nd:YAG Laser Rod," Applied Optics Vol. 9, Issue 11, pp. 2548-2553 (1970)
57. P. J. Hardman ; Optoelectron. Res. Centre, Southampton Univ., UK ; W. A. Clarkson ; G. J. Friel ; M. Pollnau," Energy-transfer upconversion and thermal lensing in high-power end-pumped Nd:YLF laser crystals," IEEE J.of Quantum Elect 35(4),647-655(1999).
58. L. Zhang, Y. G. Wang, H. J. Yu, W. Sun, Y. Y. Yang, Z. H. Han, Y. Qu, W. Hou, J. M. Li, X. C. Lin, and Y.H. Tsang, "20W high-power picosecond single-walled carbon nanotube based MOPA laser system,"IEEE J. Light. Technol.30(16), 2713-2717, (2012).
59. A. Schmidt, S. Rivier, G. Steinmeyer, J. H. Yim, W. B. Cho, S. Lee, F. Rotermund, M. C. Pujol, X. Mateos, M. Aguiló, F. Díaz, V. Petrov, and U. Griebner, "Passive mode locking of Yb:KLuW using a single-walled carbon nanotube saturable absorber," Opt. Lett. 33(7), 729-731(2008).
60. S.V. Garnov, S.A. Solokhin, E.D. Obraztsova, A.S. Lobach, P.A. Obraztsov, A.I. Chernov, V.V. Bukin, A.A. Sirotkin, Y.D. Zagumennyi, Y.D. Zavartsev, S.A. Kutovoi, and I.A. Shcherbakov,"Passive mode-locking with carbon nanotube saturable absorber in

61. M. Giuliani and W. González-Viñas," Contact-line speed and morphology in vertical deposition of diluted colloids," Phys. Rev. E 79, 032401(2009).

62. C. Jeffrey Brinker,* Yunfeng Lu, Alan Sellinger,and Hongyou Fan," Evaporation-Induced Self-Assembly:Nanostructures Made Easy," Adv. Mater., 11(7), 579-585(1999).

63. George M. Whitesides*, Bartosz Grzybowski," Self-Assembly at All Scales," Science 295(5564), 2418-2421(2002).

64. A Ulman," An Introduction to Ultrathin Organic Films: From Langmuir--Blodgett to Self--Assembly,"(2013)

65. L. Ren, C. L. Pint, L. G. Booshehri, W. D. Rice, X. Wang, D. J. Hilton, K. Takeya, I. Kawayama, M. Tonouchi, R.H. Hauge and J. Kono, "Carbon nanotube terahertz polarizer," Nano Lett., 9(7), 2610–2613(2009).

66. S. Wang , H. Yu , H. Zhang , A. Wang , M. Zhao , Y. Chen , L. Mei , and J. Wang, " Broadband Few-Layer MoS_2 Saturable Absorbers, " Adv. Mater. **26**(21), 3538–3544(2014).

67. H. Long, L. Tao, C. Y. Tang, B. Zhou, Y. D. Zhao, L. H. Zeng, S. F. Yu , S. P. Lau, Y. Chai, and Y. H. Tsang, " Tuning nonlinear optical absorption properties of WS_2 nanosheets, " Nanoscale, (2015), DOI: 10.1039/c5nr04389a.

68. B. Xu, Y. Cheng, Y. Wang, Y. Huang, J. Peng, Z. Luo, H. Xu, Z. Cai, J. Weng, and R. Moncorgé, " Passively Q-switched Nd:$YAlO_3$ nanosecond laser using MoS2 as saturable absorber, " Opt. Exp. **22**(23),. 28934-28940 (2014).

69. Y. Huang, Z. Q. Luo, Y. Y. Li, M. Zhong, B. Xu, K. J. Che, H. Y. Xu, Z. P. Cai, J. Peng, and J. Weng, "Widely tunable, passively Q-switched erbium-doped fiber laser with few-layer MoS_2 saturable absorber," Opt. Exp. **22**(21), 25258–25266 (2014).

70. H. Liu, A. P. Luo, F. Z. Wang, R. Tang, M. Liu, Z. C. Luo, W. C. Xu, C. J. Zhao, and H. Zhang, "Femtosecond pulse erbium-doped fiber laser by a few-layer MoS_2 saturable absorber," Opt. Lett. **39**(15), 4591–4594 (2014).

71. K. Wu, X. Zhang, J. Wang, X. Li, and J. Chen, "WS_2 as a saturable absorber for ultrafast photonic applications of mode-locked and Q-switched lasers ," Opt. Exp. **23**(9), 11453-11461 (2015).

72. S. H. Kassani, R. Khazaeinezhad, H. Jeong, T. Nazari, D.I. Yeom, and K. Oh, "All-fiber Er-doped Q-Switched laser based on Tungsten Disulfide saturable absorber, " Op. Mat. Exp. **5(**2), 373-379 (2015).

73. D. Mao, Y. Wang, C. Ma, L. Han, B. Jiang, X. Gan, S. Hua, W. Z. T. Mei ,and J.l. Zhao, "WS_2 mode-locked ultrafast fiber laser, " Sci. Rep. **5(**7965), 1-7 (2015).

74. M. Zhang1, G. Hu, G. Hu1, R. C. T. Howe, L. Chen, Z. Zheng, and T. Hasan, "Yb- and Er-doped fiber laser Q-switched with anoptically uniform, broadband WS2 saturableabsorber, " arXiv:1507.03188 [physics.optics]

75. Fan, Ya-Xian; He, Jing-Liang; Wang, Yong-Gang; Liu, Sheng; Wang, Hui-Tian; Ma, Xiao-Yu," 2-ps passively mode-locked Nd :YVO4 laser using an output-coupling-type semiconductor saturable absorber mirror, Appl Phys Lett, 86(10), 101103-101106(2005).